Soft genome editing based on CRISPR nickases: it takes one break to tango

Wang, Q.

Chapter 6

Selection-free precise dystrophin repair using high-capacity adenovector delivery of advanced prime editing systems rescues dystrophin synthesis in DMD muscle cells

Qian Wang[1], Sabrina Capelletti[1], Jin Liu[1], Josephine M. Janssen[1] and Manuel A.F.V. Gonçalves[1]

[1]Department of Cell and Chemical Biology, Leiden University Medical Center, Einthovenweg 20, 2333 ZC Leiden, the Netherlands

Nucleic Acids Research, 2024, Vol.52, No.5, ***2740–2757***
doi: 10.1093/nar/gkae057

ABSTRACT

Prime editors have high potential for disease modelling and regenerative medicine efforts including those directed at the muscle-wasting disorder Duchenne muscular dystrophy (DMD). However, the large size and multicomponent nature of prime editing systems pose substantial production and delivery issues. Here, we report that packaging optimized full-length prime editing constructs in adenovector particles (AdVPs) permits installing precise *DMD* edits in human myogenic cells, namely, myoblasts and mesenchymal stem cells (up to 80% and 64%, respectively). AdVP transductions identified optimized prime-editing reagents capable of restoring *DMD* reading frames of ~14% of patient genotypes and restore dystrophin synthesis and dystrophin-β-dystroglycan linkages in unselected DMD muscle cell populations. AdVPs were equally suitable for correcting DMD iPSC-derived cardiomyocytes and delivering dual prime editors tailored for *DMD* repair through targeted exon 51 deletion. Moreover, by exploiting the cell cycle-independent AdVP transduction process, we report that 2- and 3-component prime-editing modalities are both most active in cycling than in post-mitotic cells. Finally, we establish that combining AdVP transduction with seamless prime editing allows for stacking chromosomal edits through successive delivery rounds. In conclusion, AdVPs permit versatile investigation of advanced prime editing systems independently of their size and component numbers, which should facilitate their screening and application.

INTRODUCTION

Programmable nucleases consisting of sequence-tailored guide RNAs (gRNAs) and Cas9 endonucleases are powerful tools for genome editing. Yet, the prevalent repair of double-strand DNA breaks (DSB) by error-prone end joining processes confers an intrinsically high mutagenic character to nuclease-based genome editing. In contrast, prime editing permits installing any single base-pair change and precise small insertions or deletions (indels) at specific genomic sequences without DSB formation (1). Typically, prime editing complexes comprise an engineered reverse transcriptase (RT) fused to a nicking Cas9 variant (prime editor) and a 3' end-extended gRNA, named prime editing guide RNA (pegRNA). The pegRNA instructs both target site selection and an edit-of-interest via its spacer and RT template moieties, respectively. Upon target site nicking, annealing of the released single-stranded DNA to the primer binding site (PBS) of the pegRNA primes RT-mediated copying of the RNA template into a complementary DNA which, upon genomic site hybridization, flap excision, and DNA repair or replication, leads to targeted chromosomal edition (1). Prime editing has two main modalities, i.e., PE2 and PE3 (1). The former 2-component system depends solely on a prime editor protein (e.g., PE2) and a pegRNA whilst the latter 3-component system requires a supplementary regular gRNA. In PE3, gRNA-directed nicking of the non-edited DNA strand fosters its replacement by the edited strand which typically results in higher frequencies of homoduplex DNA edits despite a concomitant increase in indel by-products (1). More recently, multiplexing prime editing based on the delivery of prime editors together with dual pegRNAs is contributing to further expand the scope of DSB-independent genome editing procedures. Indeed, in this case, pairs of prime editing complexes act in concert to install genomic insertions, deletions and/or substitutions whose sizes are substantially larger than those enabled through PE2 and PE3 strategies (2-7).

Owing to their vast potential and versatility, prime editing systems are developing at a fast pace and include improved prime editor proteins and pegRNAs, e.g., PEmax (8) and engineered pegRNA (epegRNA) architectures (9,10). The PEmax construct incorporates specific mutations and codon-optimizations in its Cas9 nickase and RT portions, respectively, that contribute to enhanced prime editing activity (8). The epegRNAs have extended 3' ends in the form of structured RNA pseudoknots (e.g., tevopreQ1) that protect them from exonucleolytic degradation (9,10). Notwithstanding these important developments, the large size of prime editing components creates substantial production and delivery bottlenecks that hinder their most efficacious testing and application. Approaches aiming at ameliorating the delivery bottleneck include splitting prime editor constructs in subunits that, upon cell entry, assemble in situ tethered or untethered Cas9 nickase and RT portions (11-20). In addition, other ancillary approaches permit enriching for prime-edited cell fractions via; (i) using surrogate reporter- or drug-based systems for isolating cells co-edited at target and selectable-marker genes (21-23), or (ii) interfering with edited DNA strand removal by co-delivering dominant-negative factors of the cellular DNA mismatch repair pathway (8,10). Although applicable to specific settings, the multicomponent character of these prime-editing systems makes their design complex and their wider application challenging.

High-capacity adenoviral vector particles (AdVPs) form a powerful gene delivery system owing to their extensive packaging capacity (i.e., up to 36-kb), lack of cytotoxic viral genes, high genetic stability, and efficient transduction of dividing and post-mitotic cells (24-26). Indeed, in earlier work, our laboratory has shown that AdVPs allow for combined delivery of regular PE2 components into human cells regardless of their transformation and replication statuses (27). In this study, we investigate the potential of AdVPs for transferring optimized PE2 and PE3 components or optimized prime editing multiplexes for gene repair purposes, namely, for correcting defective *DMD* alleles underlying Duchenne muscular dystrophy (DMD). DMD (MIM #310200) is a X-linked progressive muscle-wasting disorder (incidence: ~1:5,500 boys) caused by loss-of-function mutations in the large *DMD* gene (~2.2 Mb) whose product, dystrophin (427 kDa), plays key structural and physiological roles in striated muscle (28). Interestingly, most DMD-causing mutations consist of intragenic deletions spanning single or multiple exons that disrupt the reading frame. Of notice, in-frame *DMD* deletions yield internally truncated dystrophins whose partial functionality underlies Becker muscular dystrophy (BMD) (MIM #300376), a less acute form of muscular dystrophy. Hence, restoration of the *DMD* reading frame in muscle cells is expected to result in Becker-like dystrophins with therapeutic potential (28).

We report that combining AdVP with improved prime editing systems achieves robust *DMD* gene repair and knockout in muscle progenitor cells (myoblasts) derived from DMD patients and healthy donors, respectively. Indeed, AdVP-assisted restoration of the *DMD* reading frame in human myoblasts with DMD.Δ48-50 and DMD. Δ45-50 genotypes and in induced pluripotent stem cells (iPSCs)-derived cardimyocytes with the latter genotype, readily led to the detection of Becker-like mRNA transcripts and corresponding dystrophin proteins in unselected cell populations. Importantly, proximity ligation assays revealed that the resulting Becker-like dystrophin proteins were capable of connecting to β-dystroglycan, a key member of the dystrophin-associated glycoprotein complex (DGC) present along at the sarcolemma of normal muscle cells. Complementary *DMD* gene repair experiments demonstrated the feasibility and potential of AdVP-based multiplexing prime editing involving all-in-one transfer of optimized full-length prime editor and dual pegRNA components. Moreover, AdVP transduction experiments in cycling myoblasts versus post-mitotic syncytial myotubes established that both PE2 and PE3 systems are most active in dividing cells. Finally, we explored the straightforward AdVP delivery process and the non-mutagenic character of prime editing, to build-up chromosomal edits in target cell populations through consecutive transduction cycles.

MATERIAL AND METHODS

Cells

The human iPSC line CENSOi001-B (herein named DMD iPSCs) used in this study and elsewhere (29) were generate by using an mRNA-based reprogramming protocol on fibroblasts isolated from a DMD patient with a *DMD* deletion spanning exons 45-50. These cells were purchased from the European Bank for induced pluripotent Stem Cells (EBiSC). The DMD iPSCs were maintained in mTeSR medium (STEMCELL Technologies; Cat. No.: 85850) supplemented with 25 U ml^{-1} penicillin/streptomycin (Thermo Fisher Scientific; Cat. No.: 15140122) and cultured in plates coated with Matrigel (Corning Matrigel hESC-Qualified Matrix; Corning; Cat. No.: 354277) according to the manufacturer's guidelines. When 70-80% confluence was reached, the iPSCs were washed with phosphate-buffered saline (PBS) solution (pH 7.4) and then incubated with 0.5 mM ethylenediaminetetraacetic acid (EDTA; Invitrogen Cat. No.: 15575020) in PBS at 37°C for 5 min. After the removal of the EDTA solution, the cells were seeded in mTeSR medium supplemented with a 1:200 dilution of RevitaCell (ThermoFisher Scientific; Cat. No.: A2644501).

HEK293T cells (American Type Culture Collection) were cultured in high-glucose Dulbecco's modified Eagle's medium (DMEM; Thermo Fisher Scientific; Cat. No.: 41966-029) containing 10% fetal bovine serum (FBS; Biowest; Cat. No.: S1860-500). The AdVP packaging cell line PER.tTA.Cre43 (30), was kept in high-glucose DMEM supplemented with 10% FBS, 10 mM $MgCl_2$ and 0.4 µg ml^{-1} puromycin (Thermo Fisher Scientific; Cat. No.: A11138-03). The characterization of human myoblasts derived from a healthy donor and DMD patients harboring *DMD* intragenic deletions D48–50 or D45–50, herein named, DMD.D45–50 myoblasts (KM1315), DMD.D48–50 myoblasts (AB1098) and DMD.D48–50 myoblasts (6594), have been previously detailed (31,32). These muscle progenitor cells were maintained in Ham's F-10 Nutrient Mixture (Thermo Fisher Scientific; Cat. No.: 41550-021) containing 20% heat-inactivated FBS (Thermo Fisher Scientific; Cat. No.: 10500064), 10 ng ml^{-1} recombinant

human FGF-basic (154 a.a.) (Peprotech; Cat. No.: 100-18B-500-UG), 1 μM Dexamethasone (Sigma-Aldrich; Cat. No.: D2915-100MG) and 100 U ml^{-1} penicillin/streptomycin (Thermo Fisher Scientific; Cat. No.: 15140122). The characterization and culturing of the human mesenchymal stem cells (hMSCs) was detailed elsewhere (33). In brief, these cells were kept in Minimum Essential Medium α (MEM-α) (Thermo Fisher Scientific; Cat. No.: 22561-021) supplemented with 10% FBS, 5 ng ml^{-1} recombinant human FGF-basic (154 a.a.), 100 U ml^{-1} penicillin/streptomycin, 1× non-essential amino acids (NEAA; Thermo Fisher Scientific; Cat. No.: 11140-050) and 1× GlutaMax (Thermo Fisher Scientific; Cat. No.: 35050-061). All cells were cultured at 37°C in a humidified-air 10% CO_2 atmosphere and were verified for the absence of mycoplasma.

Recombinant DNA

The generation of the various recombinant DNA constructs used in this study was done by using standard molecular cloning techniques. The annotated maps and nucleotide sequences of pegRNA expression plasmids S68_pU6.pegRNA$^{EX51.A1.RE}$, BG40_pU6.epegRNA$^{EX51.A1.RE}$, BG42_pU6.epegRNA$^{EX51.7.DEL}$ and BG43_pU6.epegRNA$^{EX51.7.INS}$, BK10_pU6.epegRNA$^{TWIN.PE}$ and the prime editor expression plasmids S65_pCAG.PE.rBGpA and BG50_pCAG.PEmax.rBGpA, are available in pages 1–16 of the **Supplementary Information**. In addition, the oligonucleotides used for the assembly of the various gRNA, pegRNA and epegRNA expression constructs are listed in **Supplementary Table S1**.

DNA transfections

The plasmid DNA transfection screens used to identify functional prime editing reagents were initiated by seeding HEK293T cells at a density of 2.0×10^5 cells per well of 24-well plates (Greiner Bio-One). After overnight incubation, the cells were transfected with the aid of 1 mg ml^{-1} 25 kDa linear polyethyleneimine (PEI, Polysciences) solution (pH 7.4) following the protocol described previously (34). The compositions of the different plasmid transfection reactions are specified in **Supplementary Tables S2** and **S3**. At 3 days post-transfection, the cells were harvested for target-site genotyping analysis.

AdVP production, purification and characterization

The production of AdVP.PE2$^{DMD.INS+1}$, AdVP.PE3$^{DMD.DEL-2}$, AdVP.PE3$^{DMD.INS+1}$ and AdVP.GpNLuc was done in bacteriophage P1 Cre recombinase-expressing PER.tTA.Cre43 cells (30) derived from the adenovirus type 5 *E1*-complementing packaging cell line PER.C6 (35). AdVP.GpNLuc encodes the reporter GpNLuc, a fusion product between EGFP and NanoLuc (36). The PER.tTA.Cre43 cells were seeded at a density of 1.8×10^6 cells per well of 6-well plates (Greiner Bio-One). The next day, the cells were transfected with 6.25 μg of MssI-linearized plasmids BG59_pAdVP.PE2$^{DMD.INS+1}$, BG62_pAdVP.PE3$^{DMD.DEL-2}$, BG63_pAdVP.PE3$^{DMD.INS+1}$, BK17_AdVP.TwinPE$^{\Delta EX51}$ or BJ03_AdVP.GpNLuc with the aid of PEI. After a 6-h incubation, the transfection medium was replaced by fresh medium containing *E1*-deleted helper AdV vector AdV.SRα.LacZ.1.50 (37) at a multiplicity of infection (MOI) of 5 transducing units (TU) per cell. The producer cells were harvested upon the emergence of complete cytopathic effect (CPE) and were then subjected to three cycles of freezing and thawing in liquid N_2 and 37°C water baths, respectively. Cellular debris were subsequently removed by centrifugation for 10 min at 2,000×g. After three rounds of propagation in PER.tTA.Cre43 cells in the presence of helper AdV.SRα.LacZ.1.50, the supernatant was harvested from twenty T175-cm^2 culture flasks (Greiner Bio-One) each containing 2.3×10^7 producer cells. Next, sequential block and continuous CsCl buoyant density ultracentrifugation was performed for purifying the vector particles present in clarified producer-cell supernatants generated after treatments with sodium deoxycholate detergent and DNaseI at 20 μg ml^{-1} (Roche; Cat. No.:10104159001). The purified vector particles were then de-salted by ultrafiltration through Amicon Ultra-15 100K MWCO filters (MerckMillipore; Cat. No:UFC910024).

Restriction enzyme fragment length analysis (RFLA) was used to determine the structural integrity of vector genomes packaged in purified adenoviral capsids. In brief, vector DNA was isolated by using the DNeasy Blood & Tissue Kit (QIAGEN; Cat. No.: 69506) with the recovered vector genomes being subsequently subjected to specific restriction enzyme digestions. The parental and helper plasmids were digested in parallel with the same restriction enzyme to serve as molecular weight references. After agarose gel electrophoresis, the digested fragments were analyzed by using the Gel-Doc XR+ system and the ImageLab (version 6.0.1) software (both from Bio-Rad). The in silico restriction patterns

corresponding to intact vector genomes and respective vector molecular clone plasmids were made with the aid of SnapGene (version 6.0.7) software.

The AdVP transducing titers were determined through quantitative PCR (qPCR) assays following previously detailed procedures (27). In brief, HeLa cells were plated at a density of 8×10^4 cells per well of 24-well plates (Greiner Bio-One). The next day, the cells were transduced with 5 serial 3-fold dilutions of each of the 100-fold diluted purified AdVP preparations. At approximately 24 h post-transduction, total cellular DNA was extracted from transduced cells via the DNeasy Blood & Tissue kit using the manufacturer's instructions. In parallel, 8 serial 10-fold dilutions of a linearized AdVP molecular clone plasmid (1×10^7 genome copies per microliter) was prepared for the generation of standard curves. Next, a qPCR specific for the AdVP DNA packaging signal was carried out on the cellular and standard curve DNA templates by using the CFX Connect Real-Time PCR Detection System (Bio-Rad) with the Bio-Rad CFX Manager (version 3.1) software being applied for data analysis. The primers, cycling conditions and components of qPCR mixtures applied are specified in **Supplementary Tables S4** and **S5**. The genome-editing AdVP MOIs indicated in this study were based on the transducing titers listed in **Supplementary Table S6**.

Muscle cell differentiation assays

Skeletal muscle cell differentiation was initiated by plating human myoblasts in 0.1% (w/v) gelatin (Sigma-Aldrich; Cat. No.: G1393) coated wells. After reaching full confluency, myoblasts were incubated in differentiation medium consisting of phenol red-free DMEM (Thermo Fisher Scientific; Cat. No.: 11880-028), 100 U ml^{-1} penicillin/streptomycin, 100 µg ml^{-1} human holo-transferrin (Sigma-Aldrich; Cat. No.: T0665) and 10 µg ml^{-1} human insulin (Sigma-Aldrich; Cat. No.: I9278). At approximately four days post-differentiation, the cultures of post-mitotic myotubes were processed for downstream analyses.

The DMD iPSCs were differentiated into beating cardiomyocytes following the protocol for cardiac lineage specification based on a stepwise supplementation of iPSC medium with specific small molecules as detailed elsewhere (38). Briefly, DMD iPSCs cultured in mTeSR medium supplemented with RevitaCell (1:200) were seeded in wells of 12-well plates coated with Matrigel at a density of $3x10^5$ cells per well. At 24 h after seeding, the culture medium was replaced by modified LI-BPEL (mBEL) medium supplemented with 5 M CHIR 99021 (Axon Medchem; Cat. No.: Axon1386) and, 48 h later, this medium was replenished by mBEL medium supplemented with 5 M XAV 939 (Tocris; Cat. No.: 3748/10) and 0.25 M IWPL6 (AbMole; Cat. No.: M2781). After two additional days, the medium was again replenished with mBEL medium, this time supplemented with Insulin-Transferrin-Selenium Ethanolamine (ITS-X) (1:1000) (Thermo Fisher; Cat. No.: 51500-056). At this stage, the cell differentiation medium was replenished every 2 days with areas of beating cardiomyocytes starting to emerge from day 10 onwards (https://doi.org/10.6084/m9.figshare.24869136). After 21 days under cardiomyogenic differentiation conditions, the cells were dissociated and processed for prime editing experiments using AdVP delivery.

Transduction experiments

The transduction of myoblasts and hMSCs was carried out as follows. Approximately 16- to 18-h prior to transduction, human myoblasts and hMSCs were seeded in 24-well plates at a density of 8×10^4 and 1×10^5 cells per well, respectively. The next day, these cells were transduced with AdVPs at the MOIs specified in the corresponding figures. Three days after transduction, the cells were transferred to a wells of 6-well plates and were sub-cultured for another seven days. Afterwards, genomic DNA from the transduced cells was isolated by using the DNeasy Blood & Tissue Kit for assessing prime-editing activities. Prime edits and bystander events in the form of indels and pegRNA scaffold-derived insertions were quantified and characterized by next-generation deep sequencing.

Experiments designed for testing the stacking of prime-editing events in target cell populations by successive transduction rounds were carried out in wild-type human myoblasts as follows. One day after seeding in 6-well plates at a density of 5×10^5 cells per well, the wild-type myoblasts were transduced with AdVP.$PE2^{DMD.INS+1}$ at an MOI of 50 TU $cell^{-1}$. After overnight incubation, the medium was substituted by fresh medium and, at three days post-transduction, fractions of myoblast suspensions were harvested for genomic DNA extraction and the remaining cell suspension bulks were seeded for a second AdVP transduction round. The same procedures were applied for the third and final AdVP

transduction round. Finally, genomic DNA samples, collected via the DNeasy Blood & Tissue Kit, were subjected to high-throughput next-generation sequencing analysis for quantifying and characterizing prime-editing events at DMD target alleles.

The comparison of prime editing activities in cycling wild-type myoblasts versus post-mitotic myotubes was initiated by seeding 5×10^4 and 2×10^5 wild-type myoblasts in wells of 24-well plates. The next day, the former cells were transduced with AdVPs at 50 TU cell^{-1} and 100 TU cell^{-1}, and the latter cells were exposed to mitogen-poor differentiation medium consisting of phenol red-free DMEM, 100 U ml^{-1} penicillin/streptomycin, 100 µg ml^{-1} human holo-transferrin and 10 µg ml^{-1} human insulin. Two days after differentiation initiation, the myotubes were treated with AdVPs at 50 TU cell^{-1} and 100 TU cell^{-1}. All the culture vessels used in this study for myotube culturing are pre-coated with 0.1% gelatin solution. AdVP-treated myoblasts and myotubes were harvested for western blotting and genomic DNA extraction at 2 and 3 days post-transduction, respectively.

Transduction experiments in DMD iPSC-derived cardiomyocytes were initiated by seeding the differentiated cardiomyocytes in wells of 96-, 48- and 24-well plates at a density of 1×10^5 cells per cm^2 in mBEL medium supplemented with ITS-X (1:1000) and a 1:200 dilution of RevitaCell. In particular, after 20 days of differentiation, the cardiomyocytes were first dissociated by incubation for 5 min at 37°C in 1× TrypLE Select (Thermo Fisher; Cat. No.: A1217701). The resulting cell suspensions were then seeded in the appropriate multi-well plates previously coated with Matrigel. Three days later, the medium was replaced by the appropriate amount of medium containing AdVPs at different MOIs and 1.5 h later, the culture medium was replenished once again. At 4 days post-transduction, the cardiomyocytes were harvested for genomic DNA analysis and, at 8 days post-transduction, they were collected for reverse transcription-qPCR (RT-qPCR) and immunofluorescence microscopy analyses. The AdVP MOI ranges applied to the myoblasts derived from different donors and to the other myogenic cell types tested, i.e. mesenchymal stem cells and iPSC-derived cardiomyocytes, did not lead to noticeable cytotoxic effects in the transduced cells.

On-target and off-target sites genotyping assays

Prime editing activities in HEK293T cells transfected with prime editing constructs were assessed through the analysis of Sanger sequencing chromatogram peaks by using the Inference of CRISPR Edits (ICE) or Tracking of Indels by Decomposition (TIDE) software packages (39,40). In brief, genomic DNA derived from treated and untreated samples was extracted with the DNeasy Blood & Tissue kit following the manufacturer's recommendations. Next, the target sites were amplified by using Phusion High-Fidelity Polymerase (Thermo Fisher Scientific; Cat. No.: #F-530L). The primer sequences, PCR mixture compositions and cycling conditions applied are listed in **Supplementary Tables S7** and **S8**. The resulting amplicons, purified by using the QIAEX II Gel Extraction Kit (QIAGEN; Cat. No.: 20021) or Mag-Bind XP beads, were then subjected to Sanger sequencing with the amplicon chromatograms derived from treated and untreated samples serving as input for TIDE or ICE analyses (39,40).

The frequencies of AdVP-induced prime edits and bystander events in the form of indels and pegRNA scaffold-derived insertions were quantified and characterized by high-throughput NGS analysis following a protocol detailed elsewhere (34). In brief, the DNeasy Blood & Tissue Kit was used to extract genomic DNA from mock-transduced myoblasts and hMSCs or from AdVP-transduced myoblasts and hMSCs and, subsequently, the extracted DNA was subjected to gene-specific PCR amplification using the Phusion High-Fidelity Polymerase. The resulting amplicons were purified with AMPure XP beads (Beckman Coulter; Cat. No.: A63881) and then were subjected to barcoding PCR. The primers, cycling parameters and PCR mixtures used for the preparation of gene-specific and barcoded amplicons are indicated in **Supplementary Tables S9-S13**. Gene-specific amplicons corresponded to the *DMD* target DNA and to the first three top-ranked candidate off-target sites for the spacer of the DMD-targeting epegRNAs. These candidate off-target sites map at an intergenic sequence of the *SLITRK5-LINC00397* locus and at intronic sequences of the *STRIP1* and *VGLL4* genes and were identified by using the CRISPOR algorithm (41). The concentrations of barcoded amplicons were measured by Qubit2.0 fluorometer (Invitrogen) with the Qubit dsDNA HS assay kit (Invitrogen; Cat. No.: Q32854) and the quality of barcoded amplicon library was assessed by 2100 Bioanalyzer system (Agilent). Finally, amplicons were pooled in equal molar ratios and subjected to next-generation Illumina MiSeq deep sequencing for obtaining 50,000 paired-end reads on a per sample basis. CRISPResso2 software (42)

was applied for data analyses after demultiplexing of the paired-end MiSeq raw reads (R1 and R2 fastq files). The quality control of the circa 50,000 paired-end reads per sample and the scripts applied for the CRISPResso2 analyses are available in the **Supplementary Information**.

Reverse transcription-qPCR

The quantification of DMD mRNA levels in unedited and AdVP-edited myoblasts was done by reverse transcription-qPCR (RT-qPCR) as follows. First, differentiation was induced in mock- and AdVP-transduced myogenic progenitor cells and, upon the formation of post-mitotic myotubes or cardiomyocytes, RNA was extracted by using the NucleoSpin RNA Kit following the manufacturer's instructions (Macherey Nagel; Cat. No.: 740955). The concentration of isolated RNA was determined by a Nanodrop apparatus and then equal amounts of RNA was reverse transcribed with the aid of the RevertAid RT Reverse Transcription Kit (Thermo Fisher Scientific; Cat. No.: K1691). In brief, 1000 ng of RNA was incubated with 0.5 µl of 100 µM random hexamer primers and 0.5 µl of 100 µM Oligo(dT)$_{18}$ primers in 12 µl reaction volumes at 65°C for 5 min followed by an 2-min incubation at 4°C. Subsequently, 1 µl of 20 U µl^{-1} RiboLock RNase Inhibitor, 1 µl of 200 U µl^{-1} RevertAid H Minus M-MuLV Reverse Transcriptase, 2 µl of 10 mM dNTP Mix and 4 µl of 5× Reaction Buffer, were directly added to each sample and the resulting mixtures were incubated at 25°C for 5 min followed by an 1-h incubation at 42°C. Afterwards, the reverse transcriptase was inactivated by heating the samples at 70°C for 5 min. The synthesized cDNA templates were then diluted 5-fold in nuclease-free water and 1 µl of the diluted cDNA template was used for qPCR amplification targeting DMD sequences with the aid of iQ™ SYBR® Green Supermix (Bio-Rad; Cat. No.: L010171C) and the primers indicated in **Supplementary Table S4**. In addition, target information, qPCR mixture components, cycling conditions and amplicon sizes are specified in **Supplementary Tables S4** and **S5**, respectively. Housekeeping *GAPDH* transcripts served as internal control target templates for gene expression normalization. The specificity of each primer pair was predicted by in silico BLAST screens and then validated with qPCR melting profile. The qPCR signal outputs were detected with the CFX Connect Real-Time PCR Detection System (Bio-Rad) and then analyzed by using the $2^{-\Delta\Delta Ct}$ method to determine the relative expression levels. Statistical analyses were done with the GraphPad Prism software (version 9.3.1).

Western blotting

Myotubes differentiated from mock- and AdVP-transduced myoblasts were lysed with Laemmli buffer consisting of 8.0% glycerol, 3% sodium dodecyl sulfate (SDS) and 200 mM Tris-HCl (pH 6.8). Protein concentrations were determined with the DC™ protein assay Kit (Bio-Rad; Cat. No.: 5000111) according to the manufacturer's protocol. Afterwards, equal amounts of proteins extracted from experimental and control samples and a dose-range of proteins extracted from healthy donor myoblasts were loaded and separated by SDS-polyacrylamide gel electrophoresis (SDS-PAGE). The loaded protein amounts and gel resolution used are specified in the corresponding figure legends. Subsequently, the resolved proteins were transferred onto 0.45-µm polyvinylidene difluoride (PVDF) membranes (Merck Millipore; Cat. No.: IPVH00010) at 60 V for 24 h, after which the membranes were blocked with 5% non-fat dry milk dissolved in Tris-buffered saline (TBS) with 0.1% Tween 20 (TBST) at room temperature (RT) for at least 1 h. Next, the membranes were incubated overnight at 4°C with the respective primary antibodies, i.e., anti-dystrophin (1:500 dilution; Abcam; Cat. No.: ab15277), anti-myosin heavy chain (1:500 dilution; Sigma-Aldrich; Cat. No.: M4276), anti-vinculin (1:1000 dilution; Sigma-Aldrich; Cat. No.: V9131), anti-GAPDH (1:1000 dilution; Merck Millipore; Cat. No.: MAB374) or anti-α/β-Tubulin (1:1000 dilution; Cell Signaling Technology; Cat. No.: 2148). After thrice washes with TBST, the membranes were probed with the appropriate secondary antibodies, i.e., anti-mouse IgG (1:5000 dilution; Sigma-Aldrich; Cat. No.: NA931V) or anti-rabbit (1:1000 dilution; Cell Signaling; Cat. No.: 7074S) at RT for 2 h. Finally, signal detection was carried out by using Clarity™ Western ECL Substrate (Bio-Rad; Cat. No.: 1705060) together with the ChemiDoc Imaging System (Bio-Rad; Cat. No.: 17001402).

Immunofluorescence microscopy analyses

Dystrophin expression in and differentiation capacity of human myoblasts subjected to AdVP-based *DMD* prime editing was assessed by immunofluorescence staining and confocal microscopy. In brief, DMD.D48–50 myoblasts (AB1098) edited via transduction with prime-editing AdVPs were incubated in myogenic differentiation medium for approximately four days and subsequently fixed with 4% paraformaldehyde (PFA), permeabilized with 0.5% Triton X-100 in TBS (50 mM Tris-HCl pH 7.5 with 100 mM NaCl) and blocked in TBS containing 0.1% Triton X-100, 2% bovine serum albumin (BSA) and

0.1% sodium azide. Cultures of unedited DMD.D48–50 myoblasts (AB1098) were equally processed in parallel Next, experimental and control specimens were incubated overnight at 4°C with the appropriate primary antibodies indicated in **Supplementary Table S14** and, after three 10-min washes with TBS, the target antigens were probed with fluorochrome-conjugated secondary antibodies (**Supplementary Table S14**). Afterwards, the specimens were mounted in ProLong Gold Antifade Mounting reagent containing DAPI (Thermo Fisher Scientific; Cat. No.: P36931). Finally, images were acquired with the aid of an upright Leica SP8 confocal microscope equipped with Leica hybrid detectors HyD and analysed with the LAS X software (Leica Microsystems). Dystrophin expression in DMD iPSC-derived cardiomyocytes that were mock-transduced or AdVP-transduced was also assessed through immunofluorescence microscopy analysis. In brief, at 8t days post-transduction, cells previously seeded in wells of 96-well plates were subjected to the above-described staining protocol except that they were incubated overnight at 4°C in blocking solution. Next, the cells exposed and not exposed to AdVP transduction were sequentially incubated for 2 h at RT with the C-terminal-specific anti-Dystrophin antibody ab15277 (Abcam), diluted 1:100, and then with the Alexa Fluor 488 goat anti-rabbit IgG (H+L) secondary antibody diluted 1:500 in TBS containing 2% BSA. The cell nuclei were stained by incubation with Hoechst 33342 (Invitrogen; Cat. No.: H3570) diluted 1:1000 in PBS for 10 min at RT. Finally, images were acquired by using a AF6000 LX microscope and subsequently analyzed with the aid of the ImageJ software (NIH, US National Institutes of Health).

Proximity ligation assays

Besides dual color fluorescence microscopy, the colocalization of dystrophin and β-dystroglycan was detected by using a proximity ligation assay (PLA). In brief, DMD.D48–50 myoblasts (AB1098 and 6594) edited via transduction with prime-editing AdVPs, were seeded in the wells of a 24-well plate containing coverslips pre-coated with 0.1% gelatin. Myogenic differentiation was triggered once the cells reached full confluence and, at approximately four days post-differentiation, the cells were fixed with 4% PFA for 10 min and permeabilized with 0.5% Triton X-100 in PBS for 5 min at RT. Subsequently, the specimens were blocked with Duolink® Blocking Solution (Sigma-Aldrich; Cat. No.: DUO82007) for 1 h at 37°C in a heated humidity chamber and were then incubated overnight at 4°C with primary antibodies against the C-terminus of dystrophin (1:100 dilution; Abcam; Cat. No.: ab15277) and β-dystroglycan (1:100 dilution; Santa Cruz Biotechnologies; Cat. No.: sc-33702) diluted in Duolink® Antibody Diluent (Sigma-Aldrich; Cat. No.: DUO82008). After three washes with Duolink® Wash Buffer A (Sigma–Aldrich; Cat. No.: DUO82046), the specimens were exposed to secondary antibodies conjugated to Duolink® PLUS and MINUS PLA probes (Sigma–Aldrich; DUO92001 and DUO92005) in Duolink® Antibody Diluent at a 1:10 dilution for 1 h at 37°C in a heated humidity chamber. Afterwards, the coverslips were washed twice with Duolink® Wash Buffer A and then exposed to Duolink® Ligase (Sigma–Aldrich; Cat. No.: DUO82027) in 1× Duolink® Ligation Buffer (Sigma–Aldrich; Cat. No.: DUO82009) at a 1:40 dilution for 30 min at 37°C in a heated humidity chamber. After two 5-min washes, the specimens were incubated with Duolink® Polymerase (Sigma–Aldrich; Cat. No.: DUO82028) in 1× Duolink® Amplification Buffer (Sigma–Aldrich; Cat. No.: DUO82011) at a 1:80 dilution for 100 min at 37°C in a heated humidity chamber. Next, the specimens were washed twice with 1× Duolink® Wash Buffer B (Sigma–Aldrich; Cat. No.: DUO82048), followed by a brief wash with 0.01× Duolink® Wash Buffer B for 1 min. Finally, the samples were mounted in VECTASHIELD Antifade Mounting Medium with DAPI (Vector Laboratories; Cat. No.: H-1200). Images were acquired by using a Leica SP8 confocal microscope equipped with Leica hybrid detectors HyD and analyzed with the LAS X software (Leica Microsystems).

Flow cytometry

The expression levels of CAR and CD46 on myoblasts from different donors were determined by using a BD LSR II flow cytometer (BD Biosciences). In brief, cells were harvested and washed with PBS supplemented with 1% BSA. Next, 1×10^5 myoblasts were resuspended in 100 µl of ice-cold PBS containing 2% BSA and then stained with 5 µl of a FITC-conjugated anti-CAR antibody (Santa Cruz Biotechnologies; Cat. No.: SC373791) or 5 µl of a PE-conjugated anti-CD46 antibody (Thermo Fisher Scientific; Cat. No.:12-0469-42) for 30 min on ice in the dark. After thrice washing with ice-cold PBS supplemented with 1% BSA, the cells were resuspended in 300 µl of PBS containing 0.5% BSA and 2 mM EDTA (pH=8.0). Myoblasts incubated with equal amounts of a FITC-conjugated IgG2b isotype control antibody (Santa Cruz Biotechnologies; Cat. No.:SC2857) or a PE-conjugated IgG1 kappa isotype control antibody (Thermo Fisher Scientific; Cat. No.:12-4714-82) served as negative controls to

establish the thresholds for background fluorescence. At least 10,000 viable single cells were acquired per sample. Data were analyzed with the aid of the FlowJo software (Tree Star; version 10.5.0).

Statistical analyses

Statistical analyses were performed with the aid of the GraphPad Prism software (version 9.3.1) on datasets derived from a minimum of three biological replicates. Two-tailed unpaired Student's t tests were carried out to analyze whether there were any statistically significant differences between two unrelated groups, whereas analysis of variance (ANOVA) was used for determining the statistical significance of three or more independent groups. One-way ANOVA and two-way ANOVA were performed on the datasets with one independent factor and two independent factors, respectively, and whenever there was a statistical significance, multiple comparison tests were followed. Dunnett's multiple comparison tests were applied for comparing each mean to a control mean, while Tukey's multiple comparison tests were used to compare each mean with each other mean. Details on statistical parameters and tests used in each experiment are specified in the respective figure legends. P values lower than 0.05 were considered to be statistically significant.

RESULTS

We started by performing transient transfection experiments in HEK293T cells for assessing the original PE2 prime editor versus the optimized PEmax variant mixed with regular pegRNAs or end-protected epegRNAs either alone (PE2 setups) or together with auxiliary gRNAs (PE3 setups). Both types of pegRNAs were designed for installing frameshifting 1-bp insertions or 2-bp deletions at *DMD* exon 51 together with 1-bp substitutions for blunting target site re-engagement through protospacer adjacent motif (PAM) elimination. Genotyping assays confirmed that epegRNAs and PEmax can foster chromosomal DNA editing (**Supplementary Figure 1**) and identified combinations of prime editing reagents designed for disrupting and restoring the *DMD* reading frame in cells with wild-type and DMD-causing genotypes, respectively (**Supplementary Figure 2**). Thus, based on these DNA transfection screens, constructs encoding optimized prime editing reagents were selected for packaging in adenoviral capsids resulting in AdVP.$^{PE2DMD.INS+1}$, for testing PE2-mediated 1-bp insertions, or in AdVP.PE3$^{DMD.INS+1}$ and AdVP.PE3$^{DMD.DEL-2}$, for testing PE3-mediated 1-bp insertions and 2-bp deletions, respectively (**Figure 1A**). Of notice, instead of prototypic adenovirus type-5 fibers, these AdVPs were endowed with type-50 fibers to, via CD46-binding, bypass the absence of the coxsackievirus and adenovirus receptor (CAR) on human myogenic cell types, namely, mesenchymal stem cells and bona fide muscle progenitors (43,44). The absence of CAR and the presence of CD46 on myoblasts derived from healthy and DMD donors was confirmed through flow cytometry analysis (**Supplementary Figure 3**). Moreover, transduction experiments with a reporter AdVP vector displaying type-50 fibers, established efficient transduction of CAR-negative muscle progenitors by CD46-binding vector particles (**Supplementary Figure 4**).

Stocks of AdVP.PE2$^{DMD.INS+1}$, AdVP.PE3$^{DMD.INS+1}$ and AdVP.PE3$^{DMD.DEL-2}$ were produced to similar high titers, i.e., 1.80×10^{10} transducing units per ml (TU ml^{-1}), 1.11×10^{10} TU ml^{-1} and 1.76×10^{10} TU ml^{-1}, respectively, and contained structurally intact vector genomes with evidence neither for rearranged nor truncated species (**Supplementary Figure 5**). Importantly, transduction experiments using prime editing CD46-targeting AdVPs in human myoblasts originated from three different DMD patients with intragenic deletions revealed a clear AdVP dose-dependent increase in the frequencies of *DMD* edition regardless of the construct used as determined by high-throughput deep sequencing (**Figure 1B** and **Supplementary Figure 6**) and inference of CRISPR edits (ICE) analyses (39) (**Supplementary Figure 7**). DMD edition upon AdVP delivery of PE3 machineries was superior to that resulting from PE2 transfer in human myoblasts (**Figure 1B** and **Supplementary Figure 6**) and, even more so, in human mesenchymal stem cells (hMSCs) used here as an independent cell type with myogenic capacity (**Supplementary Figure 8**). As expected, when compared to the PE3 machineries, PE2 led to lower frequencies of byproducts in the form of imprecise indels and epegRNA scaffold-derived insertions (**Figure 1B**, **Supplementary Figure 6** and **Supplementary Figure 8**). Interestingly, although precision indexes corresponding to edit-to-byproduct ratios were highest for PE2 complexes in human myoblasts (**Figure 1C** and **Supplementary Figure 6B**), these indexes were similar amongst PE2 and PE3 complexes in hMSCs (**Supplementary Figure 8B**). Considering that human myoblasts and hMSCs are transduced equally well by CD46-binding AdVPs (27), these data support the proposition that cell type-specific determinants, namely, complement of DNA repair factors (8,22), cell-cycle activity (22,27)

and/or target chromatin context (45), in addition to affecting the efficiency of prime editing, can also have a bearing on its ultimate product purity.

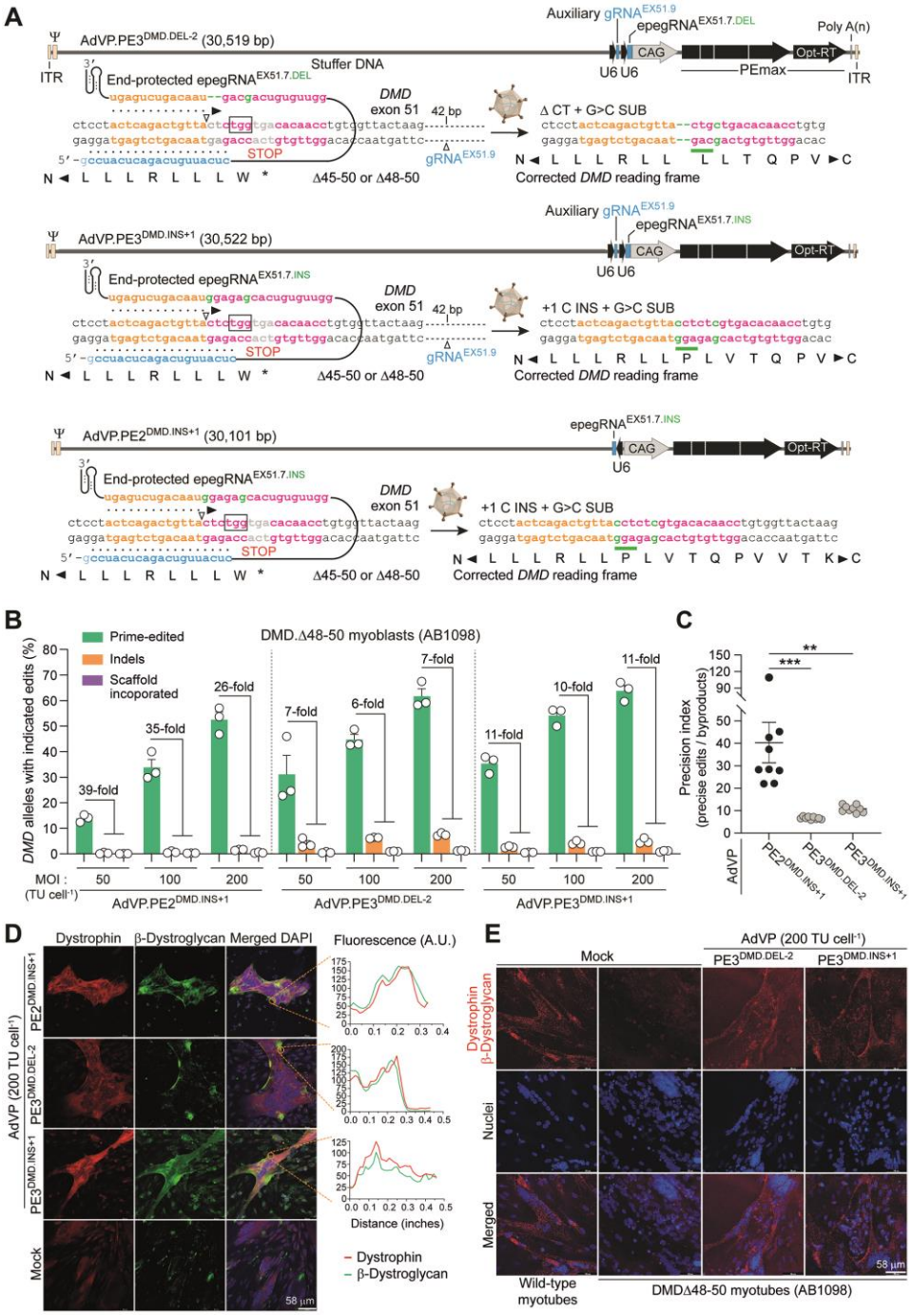

Figure 1. Gene correction through AdVP-based prime editing in *DMD* defective myoblasts. (A) Genome structures of AdVPs assembled for *DMD* prime editing. *DMD* target sequences before and after prime editing are depicted. The hybrid CAG promoter drives PEmax expression whilst the human U6 promoter controls the synthesis of the indicated epegRNAs and gRNAs. Spacer, primer binding site (PBS) and reverse transcriptase template (RTT) sequences of epegRNA are marked in cyan, orange and magenta, respectively, with encoded and installed edits labelled in green. Protospacer adjacent motifs (NGG) are boxed, and nicking positions are marked by open arrowheads. ITR and Ψ, adenovirus type-5 *cis*-acting inverted terminal repeats and packaging signal, respectively. (**B**) AdVP-based prime editing in DMD myoblasts. Human myoblasts with a Δ48-50 genotype (DMD.Δ48-50) were transduced with different multiplicities-of-infection (MOI) of AdVP.PE2$^{DMD.INS+1}$, AdVP.PE3$^{DMD.DEL-2}$ and AdVP.PE3$^{DMD.INS+1}$; TU cell^{-1}, transducing units per cell. Prime edits and unwarranted byproducts (i.e., indels and scaffold-derived insertions) were quantified by next-generation deep sequencing at 10 days post-transduction (50,000 paired-end reads per sample). Bars and error bars denote mean ± SEM, respectively, of three biological replicates. (**C**) Prime-editing precision indexes upon AdVP transduction. Precision indexes corresponding to the cumulative ratios of precise edits to byproducts frequencies measured in AdVP-transduced myoblasts DMD.Δ48-50 (AB1098) are plotted as mean ± SEM of the independent datapoints. Significances were calculated with one-way ANOVA followed by Dunnett's multiple comparison tests; ***0.0001<*P*<0.001,

0.001<*P*<0.01. (D**) Detection of dystrophin and β-dystroglycan in DMD.Δ48-50 (AB1098) muscle cells prime-edited using AdVPs. Dual-color immunofluorescence microscopy for dystrophin and β-dystroglycan was done on myotubes differentiated from DMD.Δ48-50 myoblasts transduced with the indicated DMD prime-editing AdVPs. Co-localization of dystrophin and β-dystroglycan at the plasma membrane of prime-edited DMD myotubes was assessed by image merging and dystrophin- plus β-dystroglycan-specific fluorescence signal measurements (boxed areas). Nuclei are labeled with DAPI in the merged images. (**E**) Dystrophin-β-dystroglycan interaction analysis in DMD muscle cells prime-edited using AdVPs. Proximity ligation assay detection of endogenous dystrophin-β-dystroglycan interactions was carried out on myotubes differentiated from DMD.Δ48–50 myoblasts transduced with the indicated DMD prime-editing AdVPs (red foci). Healthy donor (wild-type) and untreated DMD patient-derived myotubes served as positive and negative controls, respectively. Nuclei were labelled by DAPI staining.

Next, we sought to assess *DMD* gene expression upon myogenic differentiation of AdVP-edited DMD myoblasts. Firstly, myogenic differentiation capabilities amongst untreated and AdVP-treated myoblasts were not overtly different as probed via immunofluorescence microscopy directed at late muscle-specific markers, i.e., skeletal fast-twitch myosin heavy chain and sarcomeric a-actinin (**Supplementary Figure 9**). Secondly, consistent with *DMD* reading frame resetting, evidence for *de novo* expression of Becker-like dystrophin transcripts in differentiated myotubes was obtained via a combination of RT-qPCR assays targeting edited and unedited mRNA sequences (**Supplementary Figure 10A** and **10B**, respectively). Indeed, the latter RT-qPCR assays specific for sequences upstream and downstream of target exon 51, consistently measured a significant increase in *DMD* mRNA transcript levels in myotubes differentiated from muscle progenitors initially transduced with AdVP.PE3$^{DMD.INS+1}$ or AdVP.PE3$^{DMD.DEL-2}$ (**Supplementary Figure 10B**). Additional RT-qPCR assays specific for distal mRNA sequences encoding dystrophin C-terminal domains confirmed that, when compared to mock controls, AdVP transductions resulted in higher amounts of *DMD* mRNA transcripts in differentiated muscle cells (Supplementary Figure 11). These data indicate that DMD reading frame correction and premature stop codon elimination in prime-edited muscle cells leads to the stabilization of *DMD* transcripts presumably via an interference with otherwise operative nonsense-mediated RNA decay processes. Finally, the expression of Becker-like dystrophins was confirmed at the protein level by immunofluorescence microscopy and western blot analyses (**Figure 1D** and **Supplementary Figure 12**, respectively).

Dystrophin links the internal cytoskeleton to the DGC at the sarcolemma of striated muscle cells via binding to the transmembrane protein β-dystroglycan. In the absence of functional dystrophin molecules, and alike to other DGC proteins, β-dystroglycan presents a shorter half-life and mostly vacates the plasma membrane (46). Importantly, evidence for the stabilization and proper relocation of β-dystroglycan to the plasmalemma of differentiated AdVP-edited DMD muscle cells was provided by dual-colour confocal microscopy analysis of dystrophin and β-dystroglycan (**Figure 1D**). Moreover, proximity ligation assays (**Supplementary Figure 13**), besides independently confirming *de novo* assembly of Becker-like dystrophins in prime-edited myotubes, demonstrated the capacity of these shortened dystrophins to locally associate with β-dystroglycan (**Figure 1E** and **Supplementary Figure 14**).

Prime editing depends firstly on the complementarity of target DNA to spacer and PBS sequences in the pegRNA and, secondly, on the complementarity of the reverse transcribed template to the target sequence. As a result of these multitier hybridization requirements, prime editing at off-target positions is significantly rarer than Cas9:gRNA-induced off-target mutations in that the latter only require a single spacer-protospacer hybridization interrogation step. Nonetheless, as initially shown in a bacteriophage replication system (47), nicks can in principle also lead to mutagenic DSBs in mammalian cells if a replication fork advances through them and collapses. Indeed, earlier experiments from our laboratory using unbiased high-throughput genome-wide translocation sequencing (HTGTS) revelated that, albeit at low frequencies, Cas9 nickases do trigger chromosomal break-derived translocations involving gRNA off-target positions (34,48). Moreover, in view of the therapeutic relevance of DMD-targeting prime editing reagents, we set out to probe their specificity directly in a target cell type-of-interest (i.e., human myoblasts) by using AdVP.PE2$^{DMD.INS+1}$ and AdVP.PE3$^{DMD.INS+1}$ coupled to next-generation sequencing (NGS) analysis at the first three top-ranked candidate off-target sites, i.e., *SLITRK5*, *STRIP1* and *VGLL4* (**Figure 2A**). To increase the stringency of these genotyping assays, parallel cultures of human myoblasts were also simultaneously treated with each of the prime-editing AdVPs and a second-generation adenovector encoding the *S. pyogenes* Cas9 nuclease. These Cas9 nuclease spiking experiments maximize the chance of detecting off-target genomic modifications if the resulting Cas9:epegRNA complexes turn out to productively engage off-target sequences. NGS reads

corresponding to modified off-target sequences were mostly within background levels in cells exposed exclusively to PE2 or PE3 complexes. Importantly, in cells subjected to prime editor and Cas9 activities, modified off-target sequences were within or slightly above background levels especially at *STRIP1* where a single spacer-protospacer mismatch is identified (**Figure 2A** and **Supplementary Figure 15**). As expected, NGS reads corresponding to modified and to modified plus prime-edited target alleles (**Figure 2B**, light pink and orange sectors, respectively) were substantially higher in cells treated with Cas9 than in cells subjected exclusively to PE2 or PE3 activities (**Figure 2B**). This increase in complex on-target modifications was especially noticeable in myoblasts transduced with AdVP.PE3$^{DMD.INS+1}$, presumably due to the combined effects of coupling Cas9 to epegRNA and gRNA molecules (**Figure 2B**). Of notice, the presence of Cas9 also led to a substantial increase in the amounts of scaffold-derived indels (**Figure 2B**, light red sectors). Taken together, these data established epegRNA$^{EX51.7.INS}$ as having high specificity for DMD exon 51 while confirming the poor genotoxicity of prime editors in general (**Figure 2**).

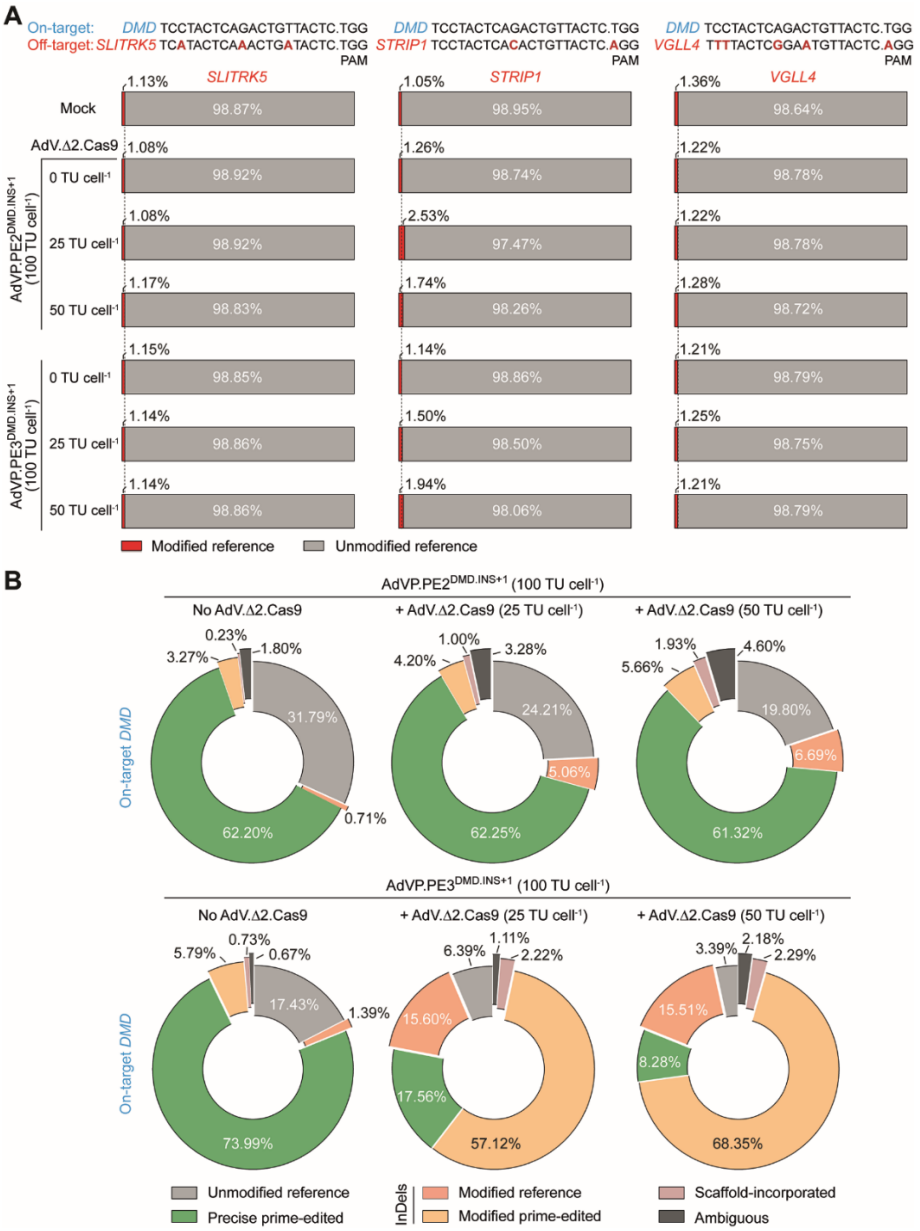

Figure 2. Assessing the specificity of *DMD* prime-editing reagents upon AdVP transduction. (A) Probing off-target activities of *DMD* prime-editing reagents. Human myoblasts DMD.Δ48-50 (AB1098) were individually transduced with AdVP.PE2$^{DMD.INS+1}$ or AdVP.PE3$^{DMD.INS+1}$ at 100 TU cell^{-1} or mixed with Cas9 nuclease-encoding vector AdV.Δ2.Cas9 at 25 TU cell^{-1} and 50 TU cell^{-1}. Genomic modifications at the top-ranked candidate off-target sites *SLITRK5*, *STRIP1* and *VGLL4* were assessed at 3 days post-transduction through NGS analysis (50,000 paired-end reads per sample). These top-ranked candidate off-target sites map at an intergenic sequence in the *SLITRK5-LINC00397* locus and at intronic sequences in the *STRIP1* and *VGLL4* genes. Nucleotide mismatches between target and off-target sites are marked in red. Mock-transduced myoblasts DMD.Δ48-50 (AB1098) provided

for negative controls. Frequencies of NGS reads corresponding to modified and unmodified off-target sequences are shown as red and grey bars, respectively. **(B)** Characterization of target *DMD* gene modifications. Genomic modifications at the *DMD* target region were also determined at 3 days post-transduction through NGS analysis (50,000 paired-end reads per sample). The different types of *DMD* gene modifications identified are indicated and distributed in the part-to-a-whole donut charts.

Nicking-based prime editing is a more predicate and less mutagenic procedure for achieving targeted gene knockouts than NHEJ-based genome editing involving CRISPR nuclease delivery and ensuing DSB formation. Hence, to complement the previous *DMD* gene correction experiments, we advanced to testing AdVP-based prime editing for establishing targeted *DMD* gene knockouts by transducing wild-type myoblasts with AdVP.PE2$^{DMD.INS+1}$ or AdVP.PE3$^{DMD.DEL-2}$ (**Figure 3A**). Interestingly, in these myoblasts, *DMD* editing levels induced by PE3 components were robust but not superior to those triggered by PE2 components (**Figure 3B**). This outcome combined with the rarity of PE2-derived indels resulted in a particularly favourable precision index for the PE2 system in these cells (**Figure 3C**). Finally, the efficient installation of frameshifting 1-bp insertions and 2-bp deletions at wild-type *DMD* alleles by AdVP.PE2$^{DMD.INS+1}$ and AdVP.PE3$^{DMD.DEL-2}$, respectively, correlated with robust gene knockout levels in transduced cells as assessed through RT-qPCR and western blot analyses (**Figure 3D** and **3E**, respectively).

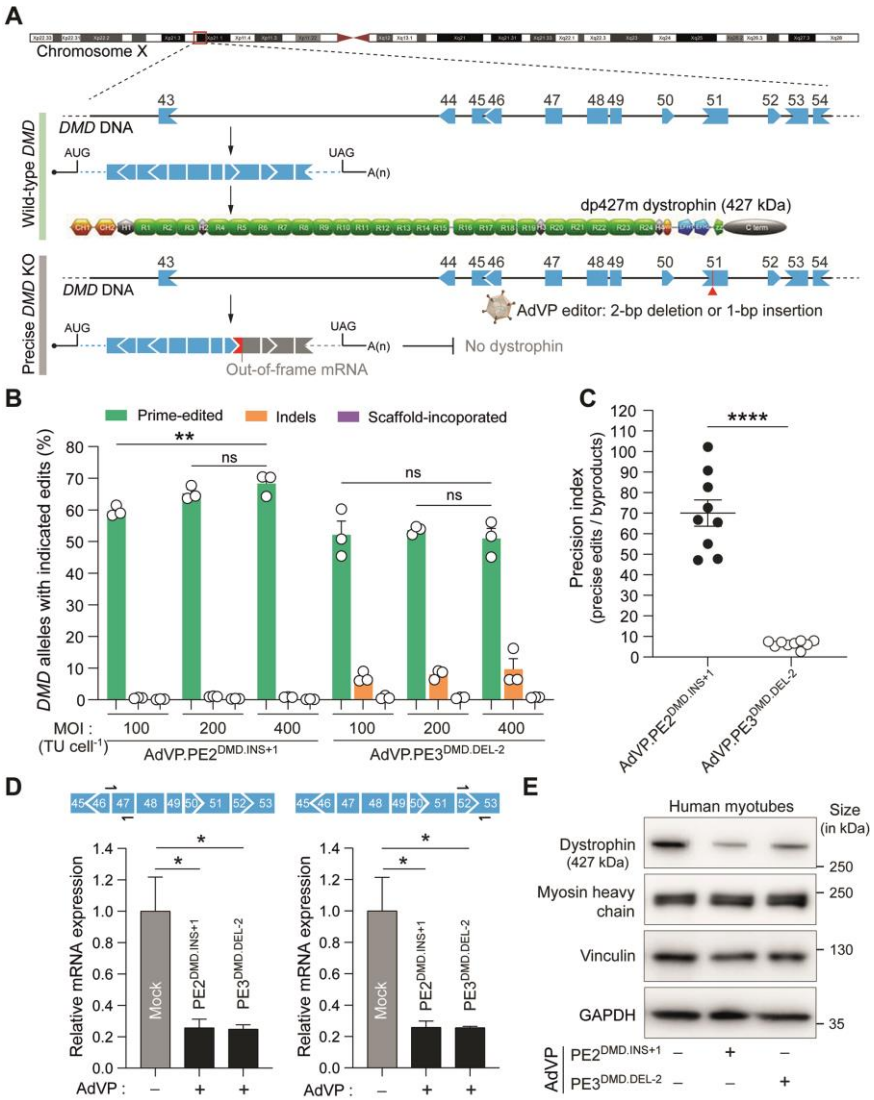

Figure 3. Gene knocking out through AdVP-based prime editing. (A) *DMD* gene knockouts using AdVP-based prime editing in human muscle cells. The synthesis and splicing of transcript isoform Dp427m leads to the assembly of 14-kb mature transcripts coding for 427-kDa dystrophin molecules whose amino and carboxy termini flank a long spectrin-like repeat region and bind to, respectively, F-actin in the cytoskeleton and dystrophin-glycoprotein complexes at the sarcolemma. In wild-type muscle cells, the installation of 2-bp deletions or 1-bp insertions within *DMD* exon 51 upon AdVP-based prime editing results in reading frame disruption and ensuing dystrophin knockout in differentiated muscle cells. (**B**) AdVP-based prime editing in wild-type myoblasts. Human myoblasts with a regular *DMD* genotype were transduced with different multiplicities-of-infection (MOI) of AdVP.PE2$^{DMD.INS+1}$, and AdVP.PE3$^{DMD.DEL-2}$; TU cell^{-1}, transducing units per cell. Prime edits and unwarranted bystander events (i.e.,

indels and scaffold-derived insertions) were measured by high-throughput NGS at 10 days post-transduction (50,000 paired-end reads per sample). Bars and error bars correspond to mean ± SEM, respectively, of three biological replicates. Significances for the indicated datasets were calculated with two-way ANOVA followed by Tukey's multiple comparison tests; **0.001<*P*<0.01; *P*>0.05 was considered non-significant (ns). (**C**) Prime-editing precision indexes upon AdVP transduction. Precision indexes corresponding to the cumulative ratios of precise edits to bystander event frequencies measured in AdVP-transduced wild-type myoblasts are plotted as mean ± SEM of the independent datapoints. Significance was calculated with the two-tailed unpaired Student's *t* test; ****P<0.0001. **(D)** Quantification of dystrophin transcripts in AdVP-edited muscle cells. RT-qPCR analysis of *DMD* expression on myotubes differentiated from human wild-type myoblasts initially transduced with AdVP.PE2$^{DMD.INS+1}$ or AdVP.PE3$^{DMD.DEL-2}$ at 400 TU per cell. Myotubes differentiated from mock-transduced myoblasts permitted measuring *DMD* mRNA steady-state levels. Significant differences between the indicated datasets were calculated with one-way ANOVA followed by Dunnett's multiple comparison tests; *0.01<*P*<0.05. Housekeeping *GAPDH* transcripts served as references for internal normalization of expression levels. **(E)** Assessing dystrophin knockout upon AdVP-based prime editing. Dystrophin western blotting was performed on myotubes differentiated from wild-type myoblasts transduced with the indicated *DMD* prime-editing AdVPs at 400 TU per cell (ten micrograms of total protein loaded per lane; 6% SDS-PAGE gel). Myotubes differentiated from mock-transduced myoblasts served as reference controls. Myogenic differentiation was controlled for by using an antibody directed to the late muscle-specific marker skeletal myosin heavy chain, and sample loading by applying antibodies recognizing vinculin and housekeeping GAPDH proteins.

By capitalizing on the cell cycle independency of adenovirus capsid-mediated delivery, we have previously found that PE2-based gene editing is, to some extent, hindered in non-cycling cells (27). To further investigate the role of the mitotic status of target cells on prime editing and, in particular, to compare PE2- versus PE3-based gene editing, AdVP.PE2$^{DMD.INS+1}$ and AdVP.PE3$^{DMD.INS+1}$ were applied to cycling myoblasts and to their post-mitotic differentiated myotube counterparts (**Figure 4A**, left panel). Western blot analysis established similar amounts of prime editor proteins in myoblasts and myotubes transduced with either AdVP.PE2$^{DMD.INS+1}$ or AdVP.PE3$^{DMD.INS+1}$ (**Figure 4A**, left panel) yet, prime editing frequencies were significantly higher in myoblasts than in myotubes regardless of whether PE2 or PE3 setups were applied (**Figure 4A**, right panel). These data support the conclusion that cell cycling favours genomic DNA editions resulting from both 2- and 3-component prime editing systems.

In contrast to cells exposed to programable nucleases, the majority of cells subjected to prime editors retain unedited alleles intact offering the possibility for additional rounds of productive prime editing to enrich for precise genome editing events within target cell populations. Hence, we next sought to explore the simple transfection-independent and non-cytotoxic AdVP delivery process to test such prime-editing stacking approach based on sequential delivery of specific prime editing complexes (**Figure 4B**, left panel). Genotyping of *DMD* target alleles in human myoblasts transduced with AdVP.PE2$^{DMD.INS+1}$ by high-throughput NGS analysis did establish the gradual build-up of prime editing events in target cell populations subjected to three consecutive AdVP transduction rounds (**Figure 4B**, right panel). Hence, precise genetic modification of cell types amenable to *in vitro* culturing might profit from AdVP-assisted prime editing stacking especially in instances where chromosomal editing frequencies reach a plateau with a single delivery round due to refractory cellular or target sequence contexts.

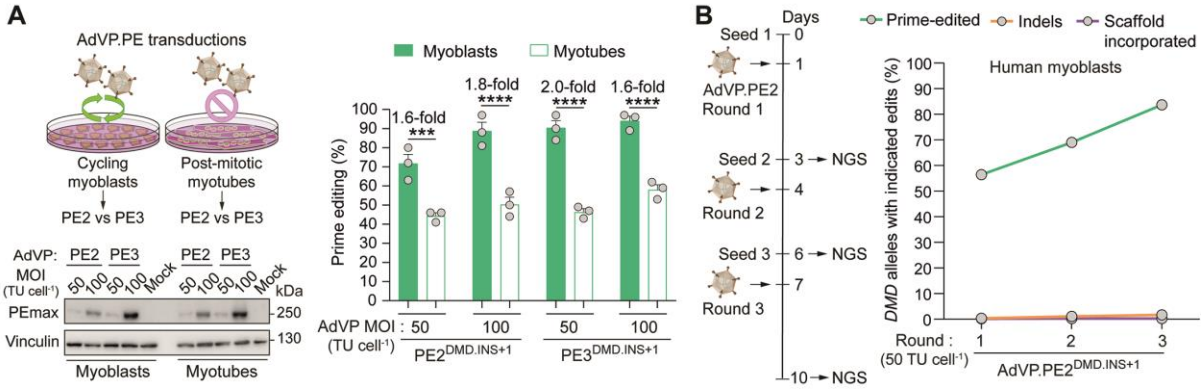

Figure 4. Assessing prime editing activities in cycling versus post-mitotic cells and upon sequential AdVP delivery. (A) Probing the impact of cell replication on PE2 versus PE3 systems. Experimental set-up and prime editor protein amounts in AdVP-transduced muscle cells (left panels). Western blot analysis of PEmax in muscle cells transduced before and after differentiation with AdVP.PE2$^{DMD.INS+1}$ and AdVP.PE3$^{DMD.INS+1}$ at 50 or 100 transducing units (TU) per cell (thirty micrograms of total protein loaded per lane; 6% SDS-PAGE gel). Cas9- and vinculin-specific antibodies detected target PEmax and loading control proteins, respectively. Prime editing frequencies in mitotic versus post-mitotic muscle cells transduced with AdVP.PE2$^{DMD.INS+1}$ and AdVP.PE3$^{DMD.INS+1}$ were quantified by inference of CRISPR edits at 3 days post-transduction. Bars and error bars denote mean ± SEM, respectively, of three biological replicates (right panel). Significances between the indicated datasets were calculated with

two-way ANOVA followed by Tukey's multiple comparison tests; ****P<0.0001, ***0.0001<P<0.001. **(B)** Probing prime editing stacking upon sequential AdVP delivery. The buildup of prime editing events in myoblast populations after three transduction rounds with AdVP.PE2$^{DMD.INS+1}$ applied at 50 transducing units (TU) per cell was quantified by high-throughput NGS at the indicated timepoints.

DMD patients often succumb to the disease due to cardiac failure (28). The integration of advanced gene editing and human iPSC technologies offers the prospect for establishing relevant disease-in-a-dish systems to investigate DMD pathological processes and candidate therapeutic agents (38). In addition, iPSCs are promising substrates for DMD-directed cell therapies owing to their self-renewal and myogenic differentiation capabilities (49-51). Hence, to test AdVP-based prime editing in an iPSC disease-modelling context, iPSCs derived from a DMD patient with a DMD.Δ45-50 genotype were first triggered to differentiate into beating cardiomyocytes (**Supplementary Files** DOI: 10.6084/m9.figshare.24869136 https://figshare.com/s/848a70783590ab572bf0). Next, the differentiated cells were either exposed or not exposed to AdVP.PE3$^{DMD.INS+1}$ and, subsequently, were subjected to *DMD* editing and expression analyses (**Figure 5A**). The former analysis revealed a clear build-up of the programmed 1-bp insertion within *DMD* exon 51 (**Figure 5B**); and, consistently with this data, the latter analysis ascertained the induction of Becker-like dystrophin expression at the mRNA and protein levels (**Figure 5C** and **5D**, respectively).

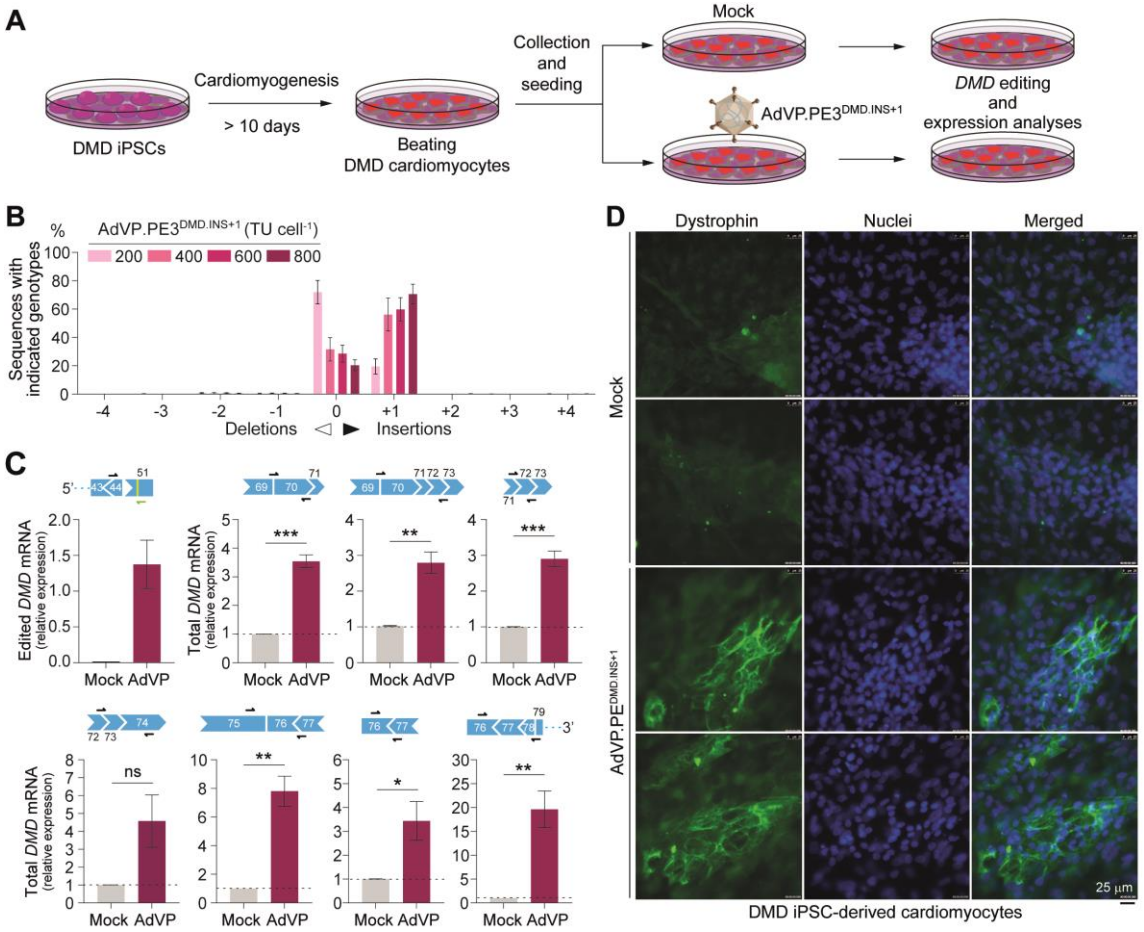

Figure 5. Testing AdVP-based prime editing in DMD iPSC-derived cardiomyocytes. (**A**) Illustration of the experimental setup. DMD iPSC-derived cardiomyocytes generated via a small-molecule differentiation protocol were transduced with prime-editing AdVP.PE3$^{DMD.INS+1}$ for endogenous *DMD* gene repair. As control, parallel cultures of differentiated cardiomyocytes were left untransduced. *DMD* editing and expression assays were performed at 4 days and 8 days post-transduction, respectively. (**B**) Quantification of prime editing. DMD iPSC-derived cardiomyocytes were transduced with AdVP.PE3$^{DMD.INS+1}$ at the indicatesd multiplicities of infection. Prime editing frequencies were determined through DNA sequencing genotyping assays at 4 days post-transduction. Bars and error bars correspond to, respectively, mean ± SEM from 3 biological replicates. (**C** and **D**) *DMD* expression analyses. RT-qPCR and fluorescence microscopy assays specific for *DMD* transcript and protein products, respectively, were done on cultures of cardiomyocytes differentiated from DMD iPSCs transduced with AdVP.PE3$^{DMD.INS+1}$ at 800 TU cell^{-1} at 8 days post-transduction. Parallel cultures of mock-transduced DMD iPSC-derived cardiomyocytes served to set *DMD* mRNA and protein baseline levels. Bars and error bars correspond to, respectively, mean ± SEM from three biological replicates. Significant differences between the indicated datasets were determined by two-tailed unpaired Student's t tests; ***0.0001 <P<0.001,**0.001<P<0.01, *0.01<P <0.05; P>0.05 was considered non-significant (ns).

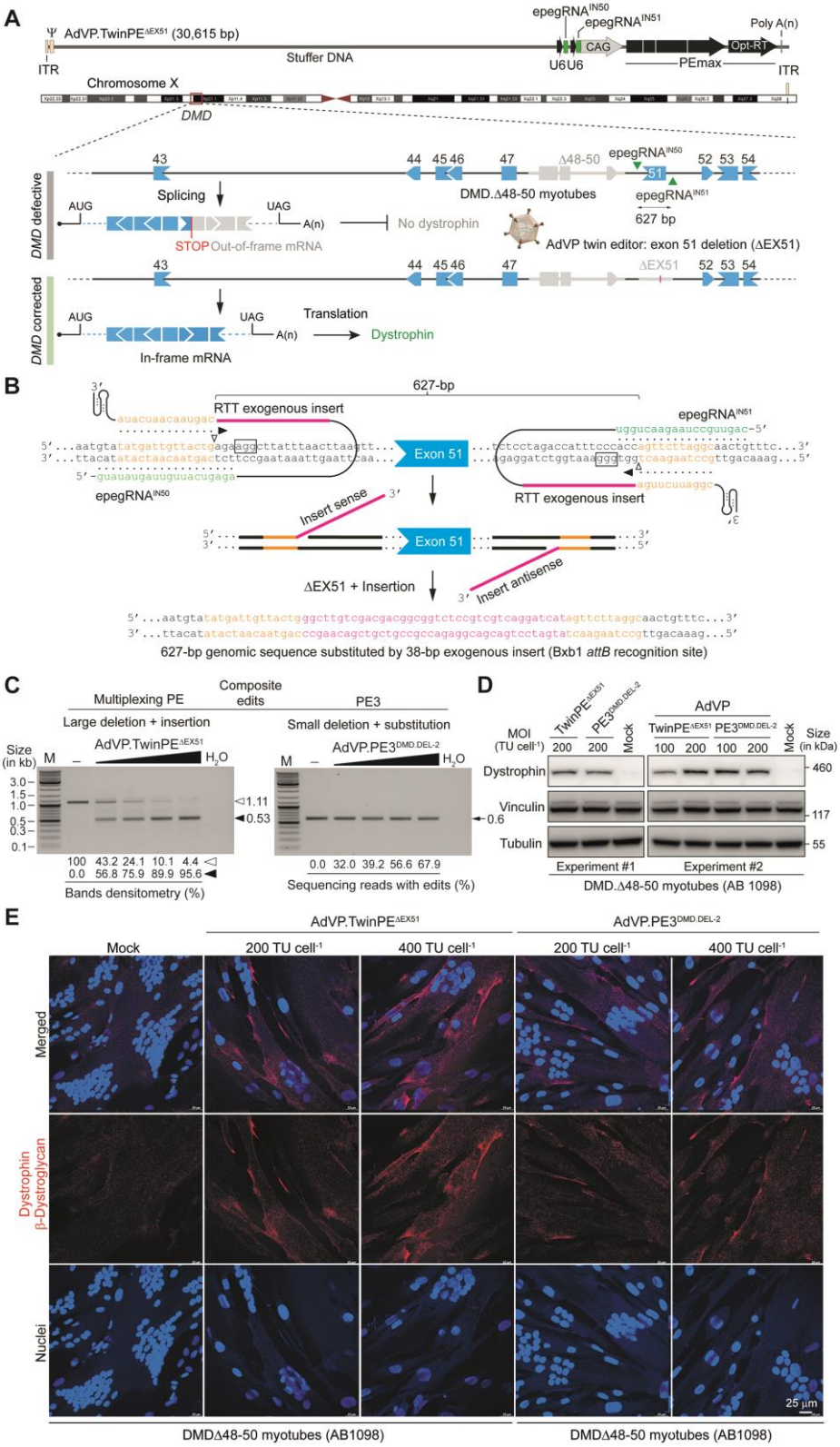

Figure 6. Gene correction through AdVP-based multiplexing prime editing in DMD defective myoblasts. (**A**) Genome structure of AdVP assembled for *DMD* gene correction using multiplexing prime editing complexes. ITR and Ψ, adenovirus type-5 cis-acting inverted terminal repeats and packaging signal, respectively. The hybrid CAG promoter drives PEmax synthesis whilst human U6 promoters drive the expression of a epegRNA pair (i.e., epegRNA^{IN50} and epegRNA^{IN51}) for *DMD* reading frame repair in muscle cells amenable to exon 51 excision (e.g., DMD.Δ48-50). (**B**) Schematics of *DMD* exon 51 excision through twin prime editing. Spacer, primer binding site (PBS) and reverse transcriptase template (RTT) sequences of epegRNA^{IN50} and epegRNA^{IN51} are highlighted in green, orange and magenta, respectively. The latter sequence encodes exogenous genetic information in the form of the serine recombinase Bxb1 *attB* recognition site. Protospacer adjacent motifs (NGG) are boxed, and nicking positions are marked by open arrowheads. Twin prime editors engage offset protospacer sequences on opposite DNA strands generating nicks that lead to the hybridization of the released single-stranded DNA strands to each PBS. The resulting free 3' hydroxyl groups

prime the synthesis of 3' DNA flaps over RTT sequences by the reverse transcriptases. After the annealing of 3' and 5' DNA flaps containing edited and original DNA sequences (not shown), respectively, removal of the 5' flaps followed by ligation of the 3' flaps to the respective DNA excising nicks yields the intended gene-editing product, i.e., replacement of genomic DNA encompassing *DMD* exon 51 by the Bxb1 *attB* recognition site. (**C**) Testing AdVP delivery of functional prime-editing multiplexes. Human myoblasts with a Δ48-50 genotype (AB1098) were transduced with AdVP.TwinPE$^{\Delta EX51}$ or AdVP.PE3$^{DMD.DEL-2}$ at 50, 100, 200 and 400 TU cell^{-1}. Twin PE- and PE3-derived prime edits were traced at 3 days post-transduction by DNA densitometry and sequencing of target DNA amplicons, respectively. (**D**) Dystrophin detection in DMD muscle cells corrected via AdVP delivery of prime-editing multiplexes. Western blotting was performed on myotubes differentiated from DMD.Δ48-50 myoblasts previously transduced with the indicated *DMD* prime-editing AdVPs (sixty micrograms of total protein loaded per lane; 6% SDS-PAGE gel). Detection of vinculin and tubulin provided for independent protein loading controls. (**E**) Dystrophin-β-dystroglycan interaction analysis in DMD muscle cells after AdVP transfer of single and dual prime-editing complexes. Detection of endogenous dystrophin-β-dystroglycan interactions by proximity ligation assays on myotubes differentiated from DMD.Δ48–50 myoblasts transduced with the indicated *DMD* prime-editing AdVPs (red foci). Parallel cultures of untreated DMD.Δ48–50 myotubes (Mock) served negative controls. Nuclei were labelled by DAPI staining.

The recent development of multiplexing prime editing strategies based on the delivery of prime editors and dual pegRNAs is contributing to further expand the scope of DSB-independent genome editing (2-7). In particular, via targeting offset target sites on opposite DNA strands and locally reverse-transcribing complementary DNA sequences, pairs of prime editing complexes are capable of yielding genomic insertions, deletions and/or substitutions whose sizes are substantially larger than those enabled via the use of PE2 and PE3 components (2-7). To investigate the feasibility and utility of AdVP-based multiplexing prime editing, the vector AdVP.TwinPE$^{\Delta EX51}$ was assembled. This vector encodes PEmax and dual epegRNAs whose "twin" arrangement (2) is designed for DMD exon 51 deletion and concomitant insertion of a recombinase recognition site (**Figure 6A** and **6B**). Of notice, most DMD-causing mutations cluster inside the exon 45-55 region (major *DMD* mutational hotspot) with the majority of these, underlying circa 13% of all DMD cases, being amenable to repair through exon 51 skipping or deletion (28) (**Figure 6B**).

Similarly to AdVPs encoding PE2 and PE3 components, AdVP.TwinPE$^{\Delta EX51}$ packaged structurally intact vector genomes (**Supplementary Figure 16**) and was produced to an high titre (i.e., 1.81×10^{10} TU ml^{-1}). Crucially, transduction experiments testing AdVP.TwinPE$^{\Delta EX51}$ next to AdVP.PE3$^{DMD.DEL-2}$ in human myoblasts with a DMD.Δ48-50 genotype, established the functionality of AdVP-delivered prime editing multiplexes via the detection of a dose-dependent accumulation of genomic edits encompassing the intended DMD exon 51 deletion (**Figure 6C** and **Supplementary Figure 17**). In fact, differentiation of DMD.Δ48-50 muscle progenitors that had been prime-edited through AdVP.TwinPE$^{\Delta EX51}$ and AdVP.PE3$^{DMD.DEL-2}$ both readily led to the detection of Becker-like dystrophins (**Figure 6D**) as well as to the assembly of protein complexes connecting these dystrophin molecules to its DGC partner β-dystroglycan (**Figure 6E**).

Taken together, these experiments support the suitability and versatility of AdVP-based prime editing for disease modelling as well as for precise gene knockout or correction in human stem/progenitor cells and their differentiated progenies.

DISCUSSION

Cell and gene therapies for DMD are under intense investigation and include the transplantation of ex vivo corrected myogenic cells and the *in vivo* delivery of RNA-guided nucleases, respectively (28,49-52). Clearly, each of these modalities have their own sets of pros and cons (49). For example, although *ex vivo* approaches offer a controlled gene repair setting and minimize immune responses to vector and gene-editing tool components, they currently present notable bottlenecks, e.g., limited cell survival and tissue engraftment (49-51). Hence, *in vivo* DMD-directed therapeutic modalities such as those based on co-administering dual AAVs encoding Cas9 nucleases and cognate gRNAs, are also being actively investigated (52). Despite the detection of immune responses against capsid and nuclease components in adult immunocompetent animals, collectively, these reports demonstrate that AAV-based *DMD* gene repair can improve striated muscle function. A potentially insidious outcome identified is, however, the prevalent integration of AAV vector DNA at site-specific DSBs, including at *Dmd* exons 51 and 53 in muscle tissues (53,54). These data stress the need to expand candidate genetic therapies to DSB-free gene editing systems as those based on base editors and prime editors. Prototypic base editors comprise a regular gRNA and a Cas9^{D10A} nickase linked to a cytidine or adenine deaminase that, upon target nucleotide deamination and subsequent DNA repair or replication, yield C→T and A→G substitutions, respectively (55-57). Owing to their dependency on regular gRNAs, it is easier designing

and identifying robust base editors than prime editors, provided that a PAM exists for placing a target nucleotide within the base editor's activity window. On the contrary, besides being more prone to off-target genomic modifications than prime editors and limited to installing single base-pair substitutions, base editors create bystander edits if non-target nucleotide(s) locate within their activity windows. Hence, the powerful and, to some extent, complementary attributes of base editing and prime editing technologies is spurring their research and development. In this context, delivery systems based on dual AAV strategies comprising two AAV vectors each encoding split portions of prime editors or base editors are being actively pursued. In cells co-transduced with split AAV vectors, prime editing or base editing ensues upon *in situ* assembly of complete proteins via intein trans-splicing dependent and independent processes (11-20). A recently optimized dual AAV prime editing system yielded up to 11% of precise gene edition in murine hearts (58). Moreover, dual AAV base editing systems were shown to, either via targeted splice site motif disruption or point mutation correction, yield *Dmd* reading frame repair and ensuing dystrophin expression in striated muscles of dystrophic mice (59,60).

Notwithstanding the amassing of important proof-of-concepts for disease modelling and gene correction, dual AAV designs are complex and require that co-transductions lead to effective and proper assembly of independent gene-editing tool parts. Recently, adenovectors deleted in early viral genes and encoding a shortened prime editor lacking the dispensable RNaseH domain, were shown to be superior to dual AAV vectors for prime editing in mouse livers (14). However, high immunogenicity *in vivo* and cytotoxicity *in vitro* is often associated with these first-generation adenoviral vectors due to their high viral gene content (24-26). Hence, there is also a pressing need to expand the range of prime editing delivery options, especially those that like AAV lack viral genes but that instead of AAV have large cargo capacities.

Towards this goal, in this study, we have established the feasibility of deploying fully viral gene-deleted AdVPs for efficient *DMD* prime editing in cell types whose myogenic capacity has supported their investigation as candidate cell therapy substrates (i.e., myoblasts, mesenchymal stem cells and iPSCs) (50-51). Indeed, combined all-in-one AdVP transfer of optimized prime-editing components in the form of PEmax (8), DMD-targeting epegRNAs (9) and auxiliary gRNAs with an improved scaffold (61), or optimized dual prime editing complexes, resulted in the robust accumulation of *DMD* edits in the form of precise small insertions or deletions or whole exon excisions. Importantly, DMD myoblasts subjected to AdVP delivery of optimized prime-editing complexes retained their myogenic differentiation capacity resulting in selection-free detection of Becker-like dystrophin molecules capable of physically associating with β-dystroglycan, a key component of the DGC (46). Moreover, gene knockout and gene repair experiments in skeletal muscle and iPSC-derived cardiac cells, respectively, have further supported AdVP-based prime editing for establishing human disease-in-a-dish models that can be directed for studying pathological processes or screening therapeutic candidates.

Despite our finding that PE2- and PE3-based gene editing is somewhat less active in post-mitotic than in cycling muscle cells, the capacity of AdVPs to efficiently transduce cells independently of their mitotic status warrants their future testing in animal models, including in humanized dystrophin-defective mice in which human DMD gene-tailored tools can be directly tested *in vivo*. Finally, we demonstrate that combining facile and non-cytotoxic AdVP transduction with non-mutagenic prime editing, permits the selective stacking of precise genome editing events in target cell populations via reiterated delivery of prime editing complexes. Such protocols might be beneficial in instances where prime editing reaches a single-dose plateau or is suboptimal due to refractory cellular or target site contexts.

Precision genome editing is increasingly underpinned by large and multicomponent tools whose testing and application using common delivery agents such as AAV is rendered complex or ineffective. Moreover, in a recent study from our laboratory investigating AdVP transfer of forced CRISPR-Cas9 heterodimers, it is demonstrated that the efficiency and accuracy of multiplexing genome editing can profit from integrated as opposed to separated delivery of the attendant reagents (62). Presumably, these improved outcomes result from the increased likelihood that integrated delivery leads to a more balanced assembly and synchronous action of otherwise individually acting CRISPR-Cas9 complexes. Hence, it is possible that other advanced multiplexing genome editing approaches will equally profit from combined all-in-one delivery systems. Amongst these systems are those based on prime editors and dual pegRNAs that, via targeting bipartite target sites on opposite strands and reverse-transcribing

complementary DNA sequences, permit deleting or replacing specific genomic tracts (2-7). Indeed, in this study, we demonstrate the value of AdVP-assisted multiplexing prime editing based on all-in-one delivery of full-length PEmax and dual epegRNAs designed for *DMD* reading frame repair through targeted exon deletion.

Finally, as aforementioned, experimental data reported elsewhere and here links prime editing performance to cell type- or cell stage-specific determinants, namely, complement of DNA repair factors (8,22), cell-cycle activity (**Figure 4**) (22,27) and/or chromatin context (45). The tropism adaptability and cell cycle independency of AdVP systems might thus facilitate probing wanted and unwanted effects of specific prime editing reagents directly on the (epi)genomes of different human cell types at mature, progenitor or undifferentiated stages.

In conclusion, combined delivery of full-length conventional and dual prime editing components in single AdVPs yields efficient and precise modification of *DMD* alleles in stem/progenitor cells with myogenic capacity. Generically, AdVPs serve as a robust and versatile platform for investigating advanced prime editing principles in difficult-to-transfect cell types independently of the size and numbers of the attendant reagents. As a corollary, AdVP-assisted prime editing warrants further research and testing, including for the modelling and repairing of genetic defects underlying human disorders in *ex vivo* and *in vivo* settings.

DATA AVAILABILITY

The data supporting this study are included in the article and accompanying supplementary files. The raw deep-sequencing library reads are deposited at the NCBI Sequence Read Archive (SRA) database under BioProject ID number: PRJNA957967. The movies illustrating light microscopy fields of beating DMD iPSC-derived cardiomyocytes are available in Figshare at https://doi.org/10.6084/m9.figshare.24869136.

ACKNOWLEDGMENTS

The authors thank Vincent Mouly (Institute of Myology, Sorbonne University, Paris, France) for providing the human myoblasts with wild-type and DMD defective genotypes and Chuannan Fan (LUMC, Department of Cell and Chemical Biology) for performing western blots. The authors are also thankful to Antoine A.F. de Vries (LUMC, Department of Cardiology) for providing a construct encoding the GpNLuc reporter. Authors of this study are members of the European Reference Network – Neuromuscular diseases (ERN EURO-NMD).

FUNDING

This research was supported by the Prinses Beatrix Spierfonds (grant number: W.OR21-01). This project has received funding from the European Union's Horizon Europe research and innovation programme under the Marie Skłodowska Curie Actions grant agreement no. 101072427 (GetRadi – Gene Therapy of Rare Diseases). Qian Wang held a Ph.D. fellowship from the China Scholarship Council–Leiden University joint scholarship programme.
Conflict of interest statement. None declared.

SUPPLEMENTARY DATA

Supplementary Data are available online at doi: 10.1093/nar/gkae057.

REFERENCES

1. Anzalone, A.V., Randolph, P.B., Davis, J.R., Sousa, A.A., Koblan, L.W., Levy, J.M., Chen, P.J., Wilson, C., Newby, G.A., Raguram, A. et al. (2019) Search-and-replace genome editing without double-strand breaks or donor DNA. Nature, 576, 149-157.
2. Anzalone, A.V., Gao, X.D., Podracky, C.J., Nelson, A.T., Koblan, L.W., Raguram, A., Levy, J.M., Mercer, J.A.M. and Liu, D.R. (2022) Programmable deletion, replacement, integration and inversion of large DNA sequences with twin prime editing. Nat Biotechnol, 40, 731-740.
3. Choi, J., Chen, W., Suiter, C.C., Lee, C., Chardon, F.M., Yang, W., Leith, A., Daza, R.M., Martin, B. and Shendure, J. (2022) Precise genomic deletions using paired prime editing. Nat Biotechnol, 40, 218-226.

4. Jiang, T., Zhang, X.O., Weng, Z. and Xue, W. (2022) Deletion and replacement of long genomic sequences using prime editing. Nat Biotechnol, 40, 227-234.
5. Tao, R., Wang, Y., Jiao, Y., Hu, Y., Li, L., Jiang, L., Zhou, L., Qu, J., Chen, Q. and Yao, S. (2022) Bi-PE: bi-directional priming improves CRISPR/Cas9 prime editing in mammalian cells. Nucleic Acids Res, 50, 6423-6434.
6. Wang, J., He, Z., Wang, G., Zhang, R., Duan, J., Gao, P., Lei, X., Qiu, H., Zhang, C., Zhang, Y. et al. (2022) Efficient targeted insertion of large DNA fragments without DNA donors. Nat Methods, 19, 331-340.
7. Zhuang, Y., Liu, J., Wu, H., Zhu, Q., Yan, Y., Meng, H., Chen, P.R. and Yi, C. (2022) Increasing the efficiency and precision of prime editing with guide RNA pairs. Nat Chem Biol, 18, 29-37.
8. Chen, P.J., Hussmann, J.A., Yan, J., Knipping, F., Ravisankar, P., Chen, P.F., Chen, C., Nelson, J.W., Newby, G.A., Sahin, M. et al. (2021) Enhanced prime editing systems by manipulating cellular determinants of editing outcomes. Cell, 184, 5635-5652.
9. Nelson, J.W., Randolph, P.B., Shen, S.P., Everette, K.A., Chen, P.J., Anzalone, A.V., An, M., Newby, G.A., Chen, J.C., Hsu, A. et al. (2022) Engineered pegRNAs improve prime editing efficiency. Nat Biotechnol, 40, 402-410.
10. Chen, P.J. and Liu, D.R. (2023) Prime editing for precise and highly versatile genome manipulation. Nat Rev Genet, 24, 161-177.
11. Liu, P., Liang, S.Q., Zheng, C., Mintzer, E., Zhao, Y.G., Ponnienselvan, K., Mir, A., Sontheimer, E.J., Gao, G., Flotte, T.R. et al. (2021) Improved prime editors enable pathogenic allele correction and cancer modelling in adult mice. Nat Commun, 12, 2121.
12. Jang, H., Jo, D.H., Cho, C.S., Shin, J.H., Seo, J.H., Yu, G., Gopalappa, R., Kim, D., Cho, S.R., Kim, J.H. et al. (2022) Application of prime editing to the correction of mutations and phenotypes in adult mice with liver and eye diseases. Nat Biomed Eng, 6, 181-194.
13. Zhi, S., Chen, Y., Wu, G., Wen, J., Wu, J., Liu, Q., Li, Y., Kang, R., Hu, S., Wang, J. et al. (2022) Dual-AAV delivering split prime editor system for in vivo genome editing. Mol Ther, 30, 283-294.
14. Bock, D., Rothgangl, T., Villiger, L., Schmidheini, L., Matsushita, M., Mathis, N., Ioannidi, E., Rimann, N., Grisch-Chan, H.M., Kreutzer, S. et al. (2022) In vivo prime editing of a metabolic liver disease in mice. Sci Transl Med, 14, eabl9238.
15. Gao, Z., Ravendran, S., Mikkelsen, N.S., Haldrup, J., Cai, H., Ding, X., Paludan, S.R., Thomsen, M.K., Mikkelsen, J.G. and Bak, R.O. (2022) A truncated reverse transcriptase enhances prime editing by split AAV vectors. Mol Ther, 30, 2942-2951.
16. She, K., Liu, Y., Zhao, Q., Jin, X., Yang, Y., Su, J., Li, R., Song, L., Xiao, J., Yao, S. et al. (2023) Dual-AAV split prime editor corrects the mutation and phenotype in mice with inherited retinal degeneration. Signal Transduct Target Ther, 8, 57.
17. Qin, H., Zhang, W., Zhang, S., Feng, Y., Xu, W., Qi, J., Zhang, Q., Xu, C., Liu, S., Zhang, J. et al. (2023) Vision rescue via unconstrained in vivo prime editing in degenerating neural retinas. J Exp Med, 220, e20220776.
18. Liu, B., Dong, X., Cheng, H., Zheng, C., Chen, Z., Rodriguez, T.C., Liang, S.Q., Xue, W. and Sontheimer, E.J. (2022) A split prime editor with untethered reverse transcriptase and circular RNA template. Nat Biotechnol, 40, 1388-1393.
19. Zheng, C., Liang, S.Q., Liu, B., Liu, P., Kwan, S.Y., Wolfe, S.A. and Xue, W. (2022) A flexible split prime editor using truncated reverse transcriptase improves dual-AAV delivery in mouse liver. Mol Ther, 30, 1343-1351.
20. Grunewald, J., Miller, B.R., Szalay, R.N., Cabeceiras, P.K., Woodilla, C.J., Holtz, E.J.B., Petri, K. and Joung, J.K. (2023) Engineered CRISPR prime editors with compact, untethered reverse transcriptases. Nat Biotechnol, 41, 337-343.
21. Levesque, S., Mayorga, D., Fiset, J.P., Goupil, C., Duringer, A., Loiselle, A., Bouchard, E., Agudelo, D. and Doyon, Y. (2022) Marker-free co-selection for successive rounds of prime editing in human cells. Nat Commun, 13, 5909.
22. Schene, I.F., Joore, I.P., Baijens, J.H.L., Stevelink, R., Kok, G., Shehata, S., Ilcken, E.F., Nieuwenhuis, E.C.M., Bolhuis, D.P., van Rees, R.C.M. et al. (2022) Mutation-specific reporter for optimization and enrichment of prime editing. Nat Commun, 13, 1028.
23. Simon, D.A., Talas, A., Kulcsar, P.I., Biczok, Z., Krausz, S.L., Varady, G. and Welker, E. (2022) PEAR, a flexible fluorescent reporter for the identification and enrichment of successfully prime edited cells. Elife, 11, e69504.

24. Gonçalves, M.A. and de Vries, A.A. (2006) Adenovirus: from foe to friend. Rev Med Virol, 16, 167-186.
25. Tasca, F., Wang, Q. and Gonçalves, M. (2020) Adenoviral vectors meet gene editing: a rising partnership for the genomic engineering of human stem cells and their progeny. Cells, 9, 953.
26. Ricobaraza, A., Gonzalez-Aparicio, M., Mora-Jimenez, L., Lumbreras, S. and Hernandez-Alcoceba, R. (2020) High-Capacity Adenoviral Vectors: Expanding the Scope of Gene Therapy. Int J Mol Sci, 21, 3643.
27. Wang, Q., Liu, J., Janssen, J.M., Tasca, F., Mei, H. and Gonçalves, M.A.. (2021) Broadening the reach and investigating the potential of prime editors through fully viral gene-deleted adenoviral vector delivery. Nucleic Acids Res, 49, 11986-12001.
28. Duan, D., Goemans, N., Takeda, S., Mercuri, E. and Aartsma-Rus, A. (2021) Duchenne muscular dystrophy. Nat Rev Dis Primers, 7, 13.
29. Tasca, F., Brescia, M., Wang, Q., Liu, J., Janssen, J.M., Szuhai, K. and Gonçalves M.A.(2022) Large-scale genome editing based on high-capacity adenovectors and CRISPR-Cas9 nucleases rescues full-length dystrophin synthesis in DMD muscle cells. Nucleic Acids Res., 50, 7761-7782.
30. Gonçalves, M.A., van der Velde, I., Janssen, J.M., Maassen, B.T., Heemskerk, E.H., Opstelten, D.J., Knaan-Shanzer, S., Valerio, D. and de Vries, A.A. (2002) Efficient generation and amplification of high-capacity adeno-associated virus/adenovirus hybrid vectors. J Virol, 76, 10734-10744.
31. Mamchaoui, K., Trollet, C., Bigot, A., Negroni, E., Chaouch, S., Wolff, A., Kandalla, P.K., Marie, S., Di Santo, J., St Guily, J.L. et al. (2011) Immortalized pathological human myoblasts: towards a universal tool for the study of neuromuscular disorders. Skelet Muscle, 1, 34.
32. Thorley, M., Duguez, S., Mazza, E.M.C., Valsoni, S., Bigot, A., Mamchaoui, K., Harmon, B., Voit, T., Mouly, V. and Duddy, W. (2016) Skeletal muscle characteristics are preserved in hTERT/cdk4 human myogenic cell lines. Skelet Muscle, 6, 43.
33. Gonçalves, M.A., Swildens, J., Holkers, M., Narain, A., van Nierop, G.P., van de Watering, M.J., Knaan-Shanzer, S. and de Vries, A.A. (2008) Genetic complementation of human muscle cells via directed stem cell fusion. Mol Ther, 16, 741-748.
34. Wang, Q., Liu, J., Janssen, J.M., Le Bouteiller, M., Frock, R.L. and Gonçalves, M. (2021) Precise and broad scope genome editing based on high-specificity Cas9 nickases. Nucleic Acids Res, 49, 1173-1198.
35. Fallaux, F.J., Bout, A., van der Velde, I., van den Wollenberg, D.J., Hehir, K.M., Keegan, J., Auger, C., Cramer, S.J., van Ormondt, H., van der Eb, A.J. et al. (1998) New helper cells and matched early region 1-deleted adenovirus vectors prevent generation of replication-competent adenoviruses. Hum Gene Ther, 9, 1909-1917.
36. Schaub, F.X., Reza, M.S., Flaveny, C.A., Li, W., Musicant, A.M., Hoxha, S., Guo, M., Cleveland, J.L. and Amelio, A.L. (2015) Fluorophore-NanoLuc BRET Reporters Enable Sensitive In Vivo Optical Imaging and Flow Cytometry for Monitoring Tumorigenesis. Cancer Res., 75, 5023-33.
37. Janssen, J.M., Liu, J., Skokan, J., Gonçalves, M.A. and de Vries, A.A. (2013) Development of an AdEasy-based system to produce first- and second-generation adenoviral vectors with tropism for CAR- or CD46-positive cells. J Gene Med, 15, 1-11.
38. Campostrini, G., Meraviglia, V., Giacomelli, E., van Helden, R.W.J., Yiangou, L., Davis, R.P., Bellin, M., Orlova, V.V. and Mummery, C.L. (2021) Generation, functional analysis and applications of isogenic three-dimensional self-aggregating cardiac microtissues from human pluripotent stem cells. Nat. Protoc.,16, 2213-2256.
39. Conant, D., Hsiau, T., Rossi, N., Oki, J., Maures, T., Waite, K., Yang, J., Joshi, S., Kelso, R., Holden, K. et al. (2022) Inference of CRISPR Edits from Sanger Trace Data. CRISPR J, 5, 123-130.
40. Brinkman, E.K., Chen, T., Amendola, M. and van Steensel, B. (2014) Easy quantitative assessment of genome editing by sequence trace decomposition. Nucleic Acids Res, 42, e168.
41. Concordet, J.P and Haeussler, M. (2018) CRISPOR: intuitive guide selection for CRISPR/Cas9 genome editing experiments and screens. Nucleic Acids Res., 46, W242-W245.
42. Clement, K., Rees, H., Canver, M.C., Gehrke, J.M., Farouni, R., Hsu, J.Y., Cole, M.A., Liu, D.R., Joung, J.K., Bauer, D.E. et al. (2019) CRISPResso2 provides accurate and rapid genome editing sequence analysis. Nat Biotechnol, 37, 224-226.
43. Knaan-Shanzer, S., van de Watering, M.J., van der Velde, I., Gonçalves, M.A., Valerio, D. and de Vries, A.A. (2005) Endowing human adenovirus serotype 5 vectors with fiber domains of species

B greatly enhances gene transfer into human mesenchymal stem cells. Stem Cells, 23, 1598-1607.
44. Gonçalves, M.A., Holkers, M., Cudre-Mauroux, C., van Nierop, G.P., Knaan-Shanzer, S., van der Velde, I., Valerio, D. and de Vries, A.A. (2006) Transduction of myogenic cells by retargeted dual high-capacity hybrid viral vectors: robust dystrophin synthesis in duchenne muscular dystrophy muscle cells. Mol Ther, 13, 976-986.
45. Park, S.J., Jeong, T.Y., Shin, S.K., Yoon, D.E., Lim, S.Y., Kim, S.P., Choi, J., Lee, H., Hong, J.I., Ahn, J. et al. (2021) Targeted mutagenesis in mouse cells and embryos using an enhanced prime editor. Genome Biol, 22, 170.
46. Matsumura, K. and Campbell, K.P. (1993) Deficiency of dystrophin-associated proteins: a common mechanism leading to muscle cell necrosis in severe childhood muscular dystrophies. Neuromuscul Disord, 3, 109-118.
47. Kuzminov, A. (2001) Single-strand interruptions in replicating chromosomes cause double-strand breaks. Proc Natl Acad Sci U S A, 98, 8241-8246.
48. Chen, X., Tasca, F., Wang, Q., Liu, J., Janssen, J.M., Brescia, M.D., Bellin, M., Szuhai, K., Kenrick, J., Frock, R.L. et al. (2020) Expanding the editable genome and CRISPR-Cas9 versatility using DNA cutting-free gene targeting based on in trans paired nicking. Nucleic Acids Res, 48, 974-995.
49. Maggio, I., Chen, X. and Gonçalves, M.A. (2016) The emerging role of viral vectors as vehicles for DMD gene editing. Genome Med, 8, 59.
50. Biressi, S., Filareto, A. and Rando, T.A. (2020) Stem cell therapy for muscular dystrophies. J. Clin. Invest., 130, 5652-5664.
51. Boyer, O., Butler-Browne, G., Chinoy, H., Cossu, G., Galli, F., Lilleker, J.B., Magli, A., Mouly, V., Perlingeiro, R.C.R., Previtali, S.C. et al. (2021) Myogenic Cell Transplantation in Genetic and Acquired Diseases of Skeletal Muscle. Front. Genet., 12, 702547.
52. Chemello, F., Bassel-Duby, R. and Olson, E.N. (2020) Correction of muscular dystrophies by CRISPR gene editing. J Clin Invest, 130, 2766-2776.
53. Nelson, C.E., Wu, Y., Gemberling, M.P., Oliver, M.L., Waller, M.A., Bohning, J.D., Robinson-Hamm, J.N., Bulaklak, K., Castellanos Rivera, R.M., Collier, J.H. et al. (2019) Long-term evaluation of AAV-CRISPR genome editing for Duchenne muscular dystrophy. Nat Med, 25, 427-432.
54. Hanlon, K.S., Kleinstiver, B.P., Garcia, S.P., Zaborowski, M.P., Volak, A., Spirig, S.E., Muller, A., Sousa, A.A., Tsai, S.Q., Bengtsson, N.E. et al. (2019) High levels of AAV vector integration into CRISPR-induced DNA breaks. Nat Commun, 10, 4439.
55. Komor, A.C., Kim, Y.B., Packer, M.S., Zuris, J.A. and Liu, D.R. (2016) Programmable editing of a target base in genomic DNA without double-stranded DNA cleavage. Nature, 533, 420-424.
56. Nishida, K., Arazoe, T., Yachie, N., Banno, S., Kakimoto, M., Tabata, M., Mochizuki, M., Miyabe, A., Araki, M., Hara, K,Y. et al. (2016) Targeted nucleotide editing using hybrid prokaryotic and vertebrate adaptive immune systems. Science, 353, aaf8729.
57. Gaudelli, N.M., Komor, A.C., Rees, H.A., Packer, M.S., Badran, A.H., Bryson, D.I. and Liu, D.R. (2017) Programmable base editing of A•T to G•C in genomic DNA without DNA cleavage. Nature, 551, 464-471.
58. Davis, J.R., Banskota, S., Levy, J.M., Newby, G.A., Wang, X., Anzalone, A.V., Nelson, A.T., Chen, P.J., Hennes, A.D., An, M. et al. (2023) Efficient prime editing in mouse brain, liver and heart with dual AAVs. Nat. Biotechnol. doi: 10.1038/s41587-023-01758-z. Online ahead of print.
59. Chemello, F., Chai, A.C., Li, H., Rodriguez-Caycedo, C., Sanchez-Ortiz, E., Atmanli, A., Mireault, A.A., Liu, N., Bassel-Duby, R. and Olson, E.N. (2021) Precise correction of Duchenne muscular dystrophy exon deletion mutations by base and prime editing. Sci. Adv., 7, eabg4910.
60. Xu, L., Zhang, C., Li, H., Wang, P., Gao, Y., Mokadam, N.A., Ma, J., Arnold, W.D. and Han, R. (2021) Efficient precise in vivo base editing in adult dystrophic mice. Nat. Commun., 12, 3719.
61. Dang, Y., Jia, G., Choi, J., Ma, H., Anaya, E., Ye, C., Shankar, P. and Wu, H. (2015) Optimizing sgRNA structure to improve CRISPR-Cas9 knockout efficiency. Genome Biol, 16, 280.
62. Tasca, F., Brescia, M., Liu, J., Janssen, J.M., Mamchaoui, K. and Gonçalves, M. (2023) High-capacity adenovector delivery of forced CRISPR-Cas9 heterodimers fosters precise chromosomal deletions in human cells. Mol Ther Nucleic Acids, 31, 746-762.